

Finite-Element Modeling and Calorimetric Measurement of Core Losses in Frequency-Converter- Supplied Synchronous Machines

Paavo Rasilo

Doctoral dissertation for the degree of Doctor of Science in Technology to be presented with due permission of the School of Electrical Engineering for public examination and debate in Auditorium S4 at the Aalto University School of Electrical Engineering (Espoo, Finland) on the 14th of December 2012 at 12 noon.

**Aalto University
School of Electrical Engineering
Department of Electrical Engineering
Research Group of Electromechanics**

Supervising professor

Antero Arkkio

Thesis advisor

D.Sc. (Tech.) Anouar Belahcen

Preliminary examiners

Dr. Wenping Cao, Newcastle University, Newcastle upon Tyne, UK

Prof. Andrew Knight, University of Alberta, Edmonton, AB, Canada

Opponent

Prof. Johan Gyselinck, Université libre de Bruxelles, Brussels, Belgium

Aalto University publication series

DOCTORAL DISSERTATIONS 159/2012

© Paavo Rasilo

ISBN 978-952-60-4886-4 (pdf)

ISSN-L 1799-4934

ISSN 1799-4934 (printed)

ISSN 1799-4942 (pdf)

<http://urn.fi/URN:ISBN:978-952-60-4886-4>

Unigrafia Oy

Helsinki 2012

Finland

Author

Paavo Rasilo

Name of the doctoral dissertation

Finite-Element Modeling and Calorimetric Measurement of Core Losses in Frequency-Converter-Supplied Synchronous Machines

Publisher School of Electrical Engineering**Unit** Department of Electrical Engineering**Series** Aalto University publication series DOCTORAL DISSERTATIONS 159/2012**Field of research** Electromechanics**Manuscript submitted** 13 August 2012**Date of the defence** 14 December 2012**Permission to publish granted (date)** 25 October 2012**Language** English **Monograph** **Article dissertation (summary + original articles)****Abstract**

This thesis deals with the modeling and measurement of core losses in salient-pole wound-field synchronous machines. A numerical iron-loss model for ferromagnetic core laminations has been implemented to be used within the 2-D finite-element (FE) analysis of electrical machines. The developed model combines existing models for eddy currents, magnetic hysteresis, and excess eddy-current losses in the laminations. These losses are globally coupled to the FE solution of the magnetic field in the 2-D cross-section of an electrical machine.

Numerical results obtained with the iron-loss model show that the hysteresis losses can be neglected from the FE field solution without a significant loss of accuracy in order to improve the convergence properties of the model and to speed up the computation. Coupling of the eddy-current losses and the related skin-effect phenomenon to the FE solution is more essential to predict the losses correctly, especially on the rotor side. The numerical model is applied to minimize the total electromagnetic losses by modifying the shape of the rotor pole shoe.

A calorimetric measurement system has been designed and built for experimental determination of the core losses. A 150-kVA synchronous generator is used as the test machine in the measurements, and its core losses are determined both with grid and inverter supply as a function of the load. Three prototype rotors identical in geometry but stacked of 0.5-mm insulated silicon-iron (Fe-Si) sheets and 1-mm and 2-mm uninsulated steel plates are used in the tests. According to the measurement results, the losses in the rotors stacked of the thicker sheets increase much more severely as a result of loading and inverter supply than those in the Fe-Si rotor.

When compared to the measurement results, the numerical model proves to estimate the core losses sufficiently, especially in the case of the 0.5-mm Fe-Si rotor. The modeling of the uninsulated laminations is found to be more challenging, since these may conduct currents also in the axial direction. The losses in the steel frame around the stator core are found to be extremely significant with voltages above the rated value. It is concluded that the 2-D model is also a suitable method to estimate the frame losses.

Keywords calorimetric measurements, core losses, finite-element methods, synchronous machines

ISBN (printed)**ISBN (pdf)** 978-952-60-4886-4**ISSN-L** 1799-4934**ISSN (printed)** 1799-4934**ISSN (pdf)** 1799-4942**Location of publisher** Espoo**Location of printing** Espoo**Year** 2012**Pages** 170**urn** <http://urn.fi/URN:ISBN:978-952-60-4886-4>

Tekijä

Paavo Rasilo

Väitöskirjan nimi

Taajuusmuuttajasyöttöisten tahtikoneiden sydänhäviöiden mallintaminen elementtimenetelmällä ja mittaaminen kalorimetrisesti

Julkaisija Sähkötekniikan korkeakoulu**Yksikkö** Sähkötekniikan laitos**Sarja** Aalto University publication series DOCTORAL DISSERTATIONS 159/2012**Tutkimusala** Sähkömekaniikka**Käsikirjoituksen pvm** 13.08.2012**Väitöspäivä** 14.12.2012**Julkaisuluvan myöntämispäivä** 25.10.2012 **Kieli** Englanti **Monografia** **Yhdistelmäväitöskirja (yhteenveto-osa + erillisartikkelit)****Tiivistelmä**

Tämä väitöskirja käsittelee avonapaisten, erillismagnetoitujen tahtikoneiden sydänhäviöiden mallintamista ja mittaamista. Levysydämen ferromagneettisten sähköteräslevyjen rautahäviöille on kehitetty numeerinen malli, jota voidaan käyttää sähkökoneiden kaksiulotteisen (2D) elementtimenetelmämallinnuksen yhteydessä. Kehitetty malli yhdistää olemassa olevat mallit levyjen pyörrevirta-, hystereesi- ja lisähäviöille. Nämä häviöt kytketään globaalisti magneetikentän elementtimenetelmäratkaisuun sähkökoneen poikkileikkauksen 2D-geometriassa.

Rautahäviömallilla saadut numeeriset tulokset osoittavat, että hystereesihäviöt voidaan jättää huomiotta kenttäratkaisussa ilman laskentatarkkuuden merkittävää huononemista. Pyörrevirtahäviöiden ja virranahdon kytkeminen ratkaisuun on oleellisempaa erityisesti roottorihäviöiden laskentatarkkuuden kannalta. Numeerista mallia sovelletaan sähkömagneettisten häviöiden minimoimiseksi roottorin napakengän muotoa muuttamalla.

Häviöiden kokeelliseksi määrittämiseksi on rakennettu kalorimetrinen mittausjärjestelmä. Testikoneena käytetään 150-kVA tahtigeneraattoria, jonka sydänhäviöt mitataan sekä verkko- että taajuusmuuttajakäytössä kuormituksen funktiona. Mittauksissa käytetään kolmea geometrialtaan identtistä prototyyppi-roottoria, jotka on ladottu 0.5-mm eristetyistä piiteräslevyistä (Fe-Si) sekä 1-mm ja 2-mm eristämättömistä teräslevyistä. Mittaustulosten perusteella paksummista teräslevyistä ladottujen roottoreiden häviöt kasvavat kuormituksen ja taajuusmuuttajasyötön vaikutuksesta huomattavasti enemmän kuin Fe-Si-roottorin häviöt.

Verrattaessa numeerisen mallin tuloksia mittaustuloksiin osoittautuu, että malli ennustaa sydänhäviöt riittävän hyvin erityisesti 0.5-mm Fe-Si-roottorin tapauksessa. Eristämättömien teräslevyjen mallintaminen on haasteellisempaa, sillä nämä saattavat johtaa virtaa myös aksiaalisuunnassa. Staattoripaketin ympärillä olevan teräsrungon häviöiden havaitaan olevan erittäin merkittävät nimellisyännitettä suuremmilla jännitteillä. 2D-mallin päätellään olevan sopiva menetelmä arvioimaan myös rungossa syntyviä häviöitä.

Avainsanat elementtimenetelmä, kalorimetriset mittaukset, sydänhäviöt, tahtikoneet**ISBN (painettu)****ISBN (pdf)** 978-952-60-4886-4**ISSN-L** 1799-4934**ISSN (painettu)** 1799-4934**ISSN (pdf)** 1799-4942**Julkaisupaikka** Espoo**Painopaikka** Espoo**Vuosi** 2012**Sivumäärä** 170**urn** <http://urn.fi/URN:ISBN:978-952-60-4886-4>

Preface

This work was carried out in the Research Group of Electromechanics at Aalto University School of Electrical Engineering, Department of Electrical Engineering between June 2008 and November 2012. I'm grateful for my supervisor Prof. Antero Arkkio and instructor Dr. Anouar Belahcen for their supervision and guidance during the research. The topic of rotor surface losses in synchronous machines was originally suggested by Juhani Mantere and Jan Westerlund from ABB Oy, Motors and Generators, Helsinki, who also provided valuable advice during the course of the work. The pre-examination of this thesis was performed by Dr. Wenping Cao and Professor Andy Knight, who are acknowledged for taking the time to review my work.

I'm grateful for the financial support from the Academy of Finland, the Walter Ahlström foundation, the Foundation of the Association of Electrical Engineers in Finland (Sähköinsinööriiliiton Säätiö), the Fortum Foundation, the Finnish Foundation for Economic and Technical Sciences (KAUTE), as well as from the Finnish Foundation for Technology Promotion.

I want to thank Dr. Frederic Tholence from ABB Corporate Research, Västerås, Sweden for performing the identification measurements for the lamination samples. Janne Kamppuri, Simo Mattila, Tapio Rauhala, John Shibutani, Olli Toivanen and Markku Väinämö from ABB Oy, Motors and Generators, Helsinki, are acknowledged for helping with the measurement arrangements as well as for providing useful knowledge during the work.

I wish to thank my ex-colleagues Dr. Emad Dlala and Dr. Jenni Pippuri for the interesting and valuable discussions related to iron-loss modeling. I'm also grateful for my other former and present colleagues for ensuring a nice working environment.

Building of the calorimetric measurement facility was a task I couldn't have handled alone. Jussi Ektström significantly contributed to the design and implementation of the system. Ari Haavisto was constantly involved with the measurement arrangements, providing essential help and knowledge during the course of the work. Also Ilkka Hanhivaara and Tomislav Žubrinić are acknowledged for their help with the measurements.

I thank my parents, my brother and my friends for their support throughout the work. Finally, I want to express my gratitude to Kati for her patience and encouragement during these years.

Espoo, November 6, 2012,

Paavo Rasilo

Contents

Preface	7
Contents	9
List of Publications	11
Author's Contribution	13
List of Symbols and Abbreviations	17
1. Introduction	23
1.1 Background	23
1.2 Definitions	24
1.3 Aim and Focus of the Thesis	25
1.4 Scientific Contribution	25
1.5 Outline of the Thesis	27
2. Review of Relevant Research	29
2.1 Core and Stray-Load Losses in Electrical Machines	29
2.1.1 Losses in Grid-Supplied Synchronous Machines	30
2.1.2 Additional Inverter Losses	31
2.2 Iron-Loss Estimation in Finite-Element Analysis	33
2.2.1 Theory and Experimental Models for Iron Losses	33
2.2.2 Physical Eddy-Current Loss Models	35
2.2.3 Modeling of Hysteresis and Excess Losses	36
2.2.4 Loss Models in Finite-Element Analysis	40
2.3 Calorimetric Measurement of Losses	43
2.3.1 Calorimetric Methods	43
2.3.2 Specific Applications	45
2.4 Summary and Conclusions	46

3. Methods	49
3.1 Iron-Loss Model	49
3.1.1 Eddy Currents	49
3.1.2 Constitutive Material Law	51
3.1.3 Model Identification	52
3.2 Electrical Machine Model	54
3.2.1 Initial State for Time-Stepping Simulations	54
3.2.2 Finite-Element Implementation of the Iron-Loss Model	56
3.2.3 Other Core-Loss Components	58
3.2.4 Numerical Details	59
3.3 Calorimetric Measurement System	60
3.3.1 System Description	60
3.3.2 Principles of Measurement	61
3.3.3 Accuracy and Error Analysis	63
4. Application and Results	65
4.1 Studied Machines and Core Materials	65
4.2 Verification of the Model at No Load and Short Circuit . . .	67
4.3 Effect of Iron Losses on the Field Solution	68
4.4 Core-Loss Studies in Synchronous Machines	71
4.5 Study of Design Improvements	74
5. Discussion and Conclusions	79
5.1 Discussion of the Methods and Results	79
5.1.1 Summary of the Findings	79
5.1.2 Significance of the Work	82
5.1.3 Engineering Considerations	83
5.2 Suggestions for Future Work	85
5.2.1 Global versus Local Coupling of Eddy Currents . . .	85
5.2.2 Eddy Currents in Uninsulated Lamination Stacks . .	85
5.2.3 Effects of Manufacturing on the Core Losses	86
5.3 Conclusions	86
References	89
Publication Errata	101
Publications	103

List of Publications

This thesis consists of an overview and of the following publications which are referred to in the text by their Roman numerals.

I Paavo Rasilo, Antero Arkkio. Modeling the Effect of Inverter Supply on Eddy-Current Losses in Synchronous Machines. In *International Symposium on Power Electronics, Electrical Drives, Automation and Motion (SPEEDAM)*, 5 pp., Pisa, Italy, June 2010.

II Paavo Rasilo, Emad Dlala, Katarzyna Fonteyn, Jenni Pippuri, Anouar Belahcen, Antero Arkkio. Model of Laminated Ferromagnetic Cores for Loss Prediction in Electrical Machines. *IET Electric Power Applications*, Vol. 5, No. 7, pp. 580-588, August 2011.

III Paavo Rasilo, Jussi Ekström, Ari Haavisto, Anouar Belahcen, Antero Arkkio. Calorimetric System for Measurement of Synchronous Machine Losses. *IET Electric Power Applications*, Vol. 6, No. 5, pp. 286-294, May 2012.

IV Paavo Rasilo, Anouar Belahcen, Antero Arkkio. Importance of Iron-Loss Modeling in Simulation of Wound-Field Synchronous Machines. *IEEE Transactions on Magnetics*, Vol. 48, No. 9, pp. 2495-2504, September 2012.

V Paavo Rasilo, Anouar Belahcen, Antero Arkkio. Effect of Rotor Pole-Shoe Construction on Losses of Inverter-Fed Synchronous Motors. In *XXth International Conference on Electrical Machines (ICEM)*, 5 pp.,

Marseilles, France, September 2012.

VI Paavo Rasilo, Anouar Belahcen, Antero Arkkio. Experimental Determination and Numerical Evaluation of Core Losses in a 150-kVA Wound-Field Synchronous Machine. Accepted for publication in *IET Electric Power Applications*, 14 pp., November 2012.

Author's Contribution

Publication I: "Modeling the Effect of Inverter Supply on Eddy-Current Losses in Synchronous Machines"

In this paper, the distribution of the additional inverter-induced eddy-current losses in the laminated core of a wound-field synchronous machine is numerically investigated. The additional losses are found to be induced mostly on the lagging edge of the rotor pole shoe and to be increased with loading.

Paavo Rasilo implemented the eddy-current loss model and wrote the paper. Antero Arkkio contributed through discussion and commenting on the paper.

Publication II: "Model of Laminated Ferromagnetic Cores for Loss Prediction in Electrical Machines"

This paper presents a numerical model for iron losses in a ferromagnetic lamination to be used with 2-D finite-element analysis of electrical machines. The theory and implementation of the model are presented and the model is identified and validated by means of measurements.

Paavo Rasilo implemented the models for the skin effect and excess losses, performed the numerical studies, and wrote the paper. Emad Dlala originally implemented the hysteresis model, while Katarzyna Fonteyn built the rotational single-sheet tester used for the identification measurements. Jenni Pippuri, Anouar Belahcen, and Antero Arkkio contributed through discussion and commenting on the paper.

Publication III: “Calorimetric System for Measurement of Synchronous Machine Losses”

This paper presents a calorimetric system designed for the measurement of the electromagnetic losses of a synchronous machine. The construction of the system, the principles of measurement, and analysis of the measurement error are presented. Some loss-measurement results at different loads are given.

Paavo Rasilo supervised the design and building of the measurement system, performed the test runs and the error analysis, and wrote the paper. Jussi Ekström made a significant contribution to building the setup and performing the calibration measurements. Ari Haavisto provided valuable knowledge about electrical and mechanical installations and participated in building of the setup. Anouar Belahcen and Antero Arkkio contributed through discussion and commenting on the paper.

Publication IV: “Importance of Iron-Loss Modeling in Simulation of Wound-Field Synchronous Machines”

In this paper, the effect of iron losses on the 2-D finite-element solution of the flux-density distribution in wound-field synchronous machines is evaluated. It is found that the hysteresis and excess losses can be neglected from the field solution without a significant loss of accuracy in order to speed up the computation. Accurate skin-effect modeling is found to be essential to predict the rotor eddy-current losses. Electric global quantities are concluded to be only slightly affected by the inclusion of the iron losses in the solution.

Paavo Rasilo performed the numerical simulations and the validation measurements and wrote the paper. Anouar Belahcen and Antero Arkkio contributed through discussion and commenting on the paper.

Publication V: “Effect of Rotor Pole-Shoe Construction on Losses of Inverter-Fed Synchronous Motors”

This paper presents a study of the effects of the rotor pole-shoe shape on the total electromagnetic losses of a wound-field synchronous machine under inverter supply. It is found that losses can be minimized by selecting a suitable pole-shoe shape and damper-winding slot dimensions. In ad-

dition, using lower-loss lamination material on the rotor side is found to have a significant effect on the total electromagnetic losses.

Paavo Rasilo performed the numerical simulations and wrote the paper. Anouar Belahcen and Antero Arkkio contributed through discussion and commenting on the paper.

Publication VI: “Experimental Determination and Numerical Evaluation of Core Losses in a 150-kVA Wound-Field Synchronous Machine”

This paper presents both measurement and simulation results for the core losses of a 150-kVA synchronous machine with three rotors stacked of different lamination materials. Both grid supply and inverter supply with 1-kHz and 6-kHz switching frequencies are studied. Both the load-dependent core losses and additional inverter losses are found to increase significantly when the sheet material is changed from 0.5-mm silicon-iron sheet to 2-mm uninsulated steel sheet. Unlike expected, however, almost equal losses are observed in the no-load operation with the rotors stacked of the 1-mm and 2-mm sheets. This is concluded to be caused either by the statistical galvanic contacts between the uninsulated laminations or by the different cutting methods used for the 1-mm and 2-mm sheets.

Paavo Rasilo performed the measurements and the numerical simulations and wrote the paper. Anouar Belahcen and Antero Arkkio contributed through discussion and commenting on the paper.

List of Symbols and Abbreviations

The following notation is used in this thesis. The notation in Publications I-VI may be different in some parts.

Symbols

\mathbf{a}	vector of nodal values of the axial component of the magnetic vector potential in the 2-D model
$\mathbf{a}_n, n = 0, \dots, N_b - 1$	vectors of nodal values of series-expansion coefficients for the axial component of the magnetic vector potential in the 2-D model
$A_n, n = 0, \dots, N_b - 1$	series-expansion coefficients for the axial component of the magnetic vector potential in the 2-D model
$\mathbf{A}_n, n = 0, \dots, N_b - 1$	series-expansion coefficients for magnetic vector potential in the 2-D model
b	local magnetic flux density (scalar) in the 1-D model
\mathbf{b}	local magnetic flux density (vector) in the 1-D model
\mathbf{B}	local magnetic flux density in the 2-D model
\hat{B}	amplitude of sinusoidal magnetic flux density
b^-	decreasing magnetic flux density
b^+	increasing magnetic flux density
\mathbf{b}_0	average magnetic flux density in the 1-D model
\mathbf{B}_0	average magnetic flux density in the 2-D model
$b_k^-, k = 1, \dots, N_{\text{rev}}$	reversal-point magnetic flux density after decreasing field

b_k^+ , $k = 1, \dots, N_{\text{rev}}$	reversal-point magnetic flux density after increasing field
\mathbf{b}_n , $n = 1, \dots, N_b - 1$	series-expansion coefficients for magnetic flux density in the 1-D model
\mathbf{B}_n , $n = 1, \dots, N_b - 1$	series-expansion coefficients for magnetic flux density in the 2-D model
c	experimental iron-loss coefficient
\mathbf{C}	constant matrix related to the skin-effect model
d	lamination thickness
\mathbf{D}	discrete curl matrix
E	Everett function
f	frequency
F	inverted Everett function
\mathbf{F}_n , $n = 0, \dots, N_b - 1$	residual vector from previous time step corresponding to the equations for the nodal values of the series-expansion coefficients for the axial component of the magnetic vector potential in the 2-D model
h	local magnetic field strength (scalar) in the 1-D model
\mathbf{h}	local magnetic field strength (vector) in the 1-D model
\mathbf{H}	local magnetic field strength in the 2-D model
h^-	decreasing magnetic field strength
h^+	increasing magnetic field strength
h_1^+	magnetic field strength of a first-order reversal point after increasing field
\mathbf{h}_{appr}	series-expansion approximation for magnetic field strength in the 1-D model
\mathbf{h}_s	surface magnetic field strength in the 1-D model
\mathbf{H}_s	surface magnetic field strength in the 2-D model
i	instantaneous value of current
\mathbf{J}	Jacobian matrix for Newton-Raphson iteration
\mathbf{K}	vector describing flux linkage in field equations
l	length of core
L	inductance
N	number of finite-element shape functions
N_b	number of skin-effect basis functions

$N_i, i = 1, \dots, N$	finite-element shape function
N_{rev}	number of reversal points
N_{sec}	number of symmetry sectors in machine cross section
N_ϕ	number of directions in vector hysteresis model
P	mechanical or active electrical power
q	heat leakage
Q	reactive power
q_m	mass flow
\mathbf{r}	residual vector for Newton-Raphson iteration
R	resistance
\mathbf{S}	magnetic stiffness matrix
t	time
u	instantaneous value of voltage
\mathbf{u}	unit vector
\mathbf{u}_{ϕ_i}	unit vector in direction ϕ_i
x	cross-sectional coordinate
y	cross-sectional coordinate
z	axial coordinate
$\alpha_n, n = 0, \dots, N_b - 1$	basis function for magnetic flux density
α_r	rotor angle
β	parameter describing the shape of first-order reversal curves
$\beta_n, n = 0, \dots, N_b - 1$	basis function for magnetic field strength
γ	hysteresis operator
Δh	enthalpy increase
ΔQ	rate of change of thermal energy
Δt	time-step length
μ	Preisach distribution function
ρ	mass density
σ	electrical conductivity
$\sqrt{\sigma G V_0 S}$	excess-loss coefficient
ω	angular frequency
Ω	2-D solution domain
$\Omega_{\text{db},n}$	regions of the 2-D solution domain belonging to the n^{th} damper bar
Ω_{Fe}	laminated regions of the 2-D solution domain

Subindices

The following subindices are used in combination with the variables of the previous list. If several subindices are used for one variable, these are separated by a comma (,).

b	balance test
db	damper bar
cl	classical (loss)
Cu	copper (loss)
d	direct axis
ew	end winding
ex	excess (loss)
f	field winding
Fe	iron (loss)
fw	friction and windage (loss)
hy	hysteresis (loss) / hysteretic
in	input / inlet
maj,-	decreasing branch of major hysteresis loop
maj,+	increasing branch of major hysteresis loop
out	output / outlet
q	quadrature axis
r	rotor
ref	reference
s	stator
sat	saturation
sv	single-valued
t	test run
x	x component / x direction
xy	x-y plane
y	y component / y direction
z	z component / z direction

Abbreviations

1-D	one-dimensional
2-D	two-dimensional
3-D	three-dimensional

CSU	combined standard uncertainty
D-end	drive end
DOL	directly-on-line connected
DR	differential reluctance
DTC	direct torque control
FCT	fast cosine transform
Fe-Si	silicon iron
FE	finite element
FEM	finite-element method
FORC	first-order reversal curve
FP	fixed-point (method)
JA	Jiles-Atherton (model)
N-end	non-drive end
NR	Newton-Raphson (method)
PWM	pulse-width modulation
SV	single-valued
VSD	variable-speed drive

1. Introduction

1.1 Background

Synchronous machines have been manufactured for over 100 years. During the last decades of the 20th century, when static power converters started to achieve higher power ratings, many synchronous machine manufacturers also began to provide machines for variable-speed drives (VSD). As a result of their relative good efficiencies and ability to supply reactive power, synchronous motors are typically used in high-power low-speed drive applications, such as rolling mills, mine hoists, extruders, electric propulsion, etc. Although continuous speed control can provide significant energy savings for such applications, the distorted output voltages of the power-electronic inverters increase the power losses of the machines when compared to a purely sinusoidal supply.

Power losses in electrical machines occur due to mechanical friction, the resistances of the current-conducting windings, non-zero electrical conductivities of the iron core and the support structures, as well as ferromagnetic hysteresis. For synchronous machines, standards usually divide the losses into mechanical losses, resistive losses of the armature windings, resistive losses of the excitation windings, core losses, and additional load losses or stray-load losses (IEC/EN 60034-2:2007, IEEE Std 115-1994). All the electromagnetic loss components may be affected by the nonsinusoidal supply voltage.

Because of the direct-current (DC) excitation of synchronous machines, the fundamental rotor flux does not induce any losses in the rotor core. Thus the rotors of synchronous generators and directly-on-line connected (DOL) synchronous motors have traditionally been stacked of relatively thick laminations to reduce manufacturing costs. For example, unindu-

lated 2-mm steel laminations with no added silicon contents are generally used as the rotor material of such machines. However, when a similar construction is used for an inverter-supplied machine, the highly distorted air-gap flux density induces significant eddy currents in these thick and highly conductive laminations causing excessive additional losses when compared to grid supply. This makes the wound-field synchronous machine an especially interesting application when the additional inverter losses are to be studied.

To meet the constantly tightening efficiency requirements, accurate methods are needed to predict the aforementioned losses already at the design stage. Fortunately, increasing computation performance allows more and more advanced calculation tools to be developed and to be used in everyday machine design. Typical requirements for such design tools are sufficient accuracy but, at the same time, fast performance and a simple identification process for the required parameters. This thesis aims to contribute to this area by developing a numerical calculation tool to estimate the iron losses of electrical machines. The emphasis will be on computational efficiency and the simplicity of the identification process, and applicability to synchronous machine design will be constantly ensured. In addition, measurements will be performed in order to obtain experimental knowledge on the core losses of frequency-converter-supplied synchronous machines.

1.2 Definitions

Throughout this thesis, the term *core loss* will be used to denote all possible components of power losses that are included in the total electromagnetic losses of a synchronous machine, but not in the resistive losses of the armature and field windings calculated using their DC resistances and effective currents. Therefore, in addition to the iron loss, the core loss will include the losses in the damper winding, the eddy currents and circulating currents in the armature winding, and the losses in the frame and other support structures.

The load-dependent core losses will not be considered as a separate loss component and the term *stray-load loss* will be avoided in the chapters following the background study. By *additional inverter loss* or simply *additional loss*, the increase in the power losses caused by changing from sinusoidal to inverter supply will be meant.

To make a distinction between the macroscopic eddy currents and the microscopic excess eddy currents, the term *classical loss* or *classical eddy-current loss* will be used to denote the total macroscopic eddy-current loss calculated from the flux-density distribution in the lamination. It is emphasized, that the term *classical* will not be used to denote any assumptions about the skin effect, as is sometimes done in the literature.

1.3 Aim and Focus of the Thesis

The aim of this work is to develop and apply methods for the modeling and measurement of core losses in frequency-converter-supplied synchronous machines. From the modeling point of view, the focus will be kept on the calculation of iron losses, which has remained a challenge throughout the history of electrical machines. The first goal is to develop a physical, accurate, easily identifiable, and well-convergent iron-loss model that can be coupled to a 2-D finite-element (FE) software for the numerical analysis of electrical machines. Once implemented, the model will be applied to evaluate the effect of the iron losses on the field solution of wound-field synchronous machines. The distribution of the additional inverter losses in synchronous motors will be analyzed, and some design improvements will be proposed.

A 150-kVA 4-pole synchronous machine will be used as the a test device for experimental verification of the model. The goal of the measurements is to obtain sufficient accuracy to distinguish the differences between the core losses obtained with three prototype rotors stacked of different lamination materials: a 0.5-mm silicon-iron (Fe-Si) sheet and 1-mm and 2-mm steel sheets, respectively. For this purpose, a calorimetric system will be designed and built.

1.4 Scientific Contribution

The scientific contributions of this thesis can be summarized as follows:

- A comprehensive iron-loss model for ferromagnetic laminations is developed by combining models for eddy currents, magnetic hysteresis, and excess losses.

- The iron-loss model is coupled to a 2-D FE model of electrical machines. A computationally efficient 2-D model is obtained by directly and globally coupling the lamination eddy currents to the 2-D solution of the average flux density. Excellent convergence is obtained with the Newton-Raphson (NR) method despite the hysteretic material properties.
- An iterative procedure is implemented to obtain a specific electrical operating point as the initial state for the time-stepping FE simulations. The initial state is iterated with a static FE solver combined with a two-axis model by adjusting the rotor angle and the field voltage until the desired active and reactive powers are achieved. The iteration is performed with the NR method by calculating the Jacobian matrix numerically at each iteration step.
- The effect of the iron losses on the global performance of frequency-converter-supplied synchronous motors is studied by means of numerical simulations. Suitable parameters for the iron-loss model are determined to obtain sufficient accuracy and a reasonable computation time.
- A calorimetric measurement system is designed and built to determine the total electromagnetic losses of a 150-kVA synchronous machine. Comprehensive theoretical error analysis is performed to determine the measurement error. An error of approximately 1.9 % is obtained at the rated-load operation for both grid and inverter supplies.
- The eddy-current losses in the frame of the 150-kVA machine are studied by means of both measurements and 2-D FE simulations. The frame losses are found to be extremely significant at voltages above the rated value. Despite its simplifying assumptions and the material properties of the frame not being known accurately, the 2-D FE model is found to be a sufficient tool to estimate the losses in the frame.
- The effect of the rotor lamination material on the core losses of synchronous machines is determined by means of both measurements and numerical simulations. Three prototype rotors stacked of 0.5-mm in-

sulated Fe-Si sheets and 1-mm and 2-mm uninsulated steel sheets, respectively, are tested and used in the simulations. The losses in the thicker laminations are found to be affected significantly more as a result of loading and inverter supply than those in the 0.5-mm Fe-Si sheets.

- At no-load operation, the losses measured with the rotors stacked of the 1-mm and 2-mm laminations are found to be almost equal. Since this may imply that these stacks behave more like solid conductors, the average resistivities over the stacks are measured. However, these axial resistivities are found to be around 1000 times larger than the resistivities of the materials.
- The effect of the rotor pole-shoe construction on the total electromagnetic losses of frequency-converter-supplied synchronous motors is studied by means of numerical simulations. Some possibilities for design improvements are suggested.

1.5 Outline of the Thesis

This thesis is divided into five chapters. The current chapter has provided a brief introduction to the topic of this thesis. In order to benchmark the methods and results of this work, Chapter 2 will review some relevant literature on modeling and the measurement of losses in synchronous machines. Chapter 3 will describe the methods, i.e., the numerical loss-calculation tools and the calorimetric measurement system used in this work. Chapter 4 will present the results of applying these methods to study the losses in frequency-converter-supplied synchronous machines. Finally, the work is discussed and concluded in Chapter 5.

2. Review of Relevant Research

In this chapter, a background study on the fields related to the topic of this thesis is provided. First, general theory and methods for modeling core and stray-load losses in electrical machines are reviewed. Whenever possible, the focus is kept on wound-field synchronous machines. However, the additional inverter losses in synchronous machines have not been very widely studied before and thus other applications will also be considered. The FE modeling of iron losses is a major part of this work and will thus be reviewed more deeply in the following section. Finally, existing methods for the measurement of losses are investigated. After a brief review of the relevant history of each topic, the focus is kept on contemporary results in order to benchmark the current work.

2.1 Core and Stray-Load Losses in Electrical Machines

Power losses have been of interest since the early days of electrical machines. Before numerical analysis tools were available or became commonly used, analytical methods were used for loss estimation, and experimental methods were used to identify and validate the developed models. When dealing with synchronous machines, most of the efforts have been put into modeling the stray-load losses and the losses induced on the rotor surface by the stator slot ripple and the nonsinusoidal air-gap magnetomotive force. The latter are often called *pole-surface* or *pole-face losses* and practically comprise the rotor proportion of the stray-load loss (Richardson 1945).

More recently, the finite-element method (FEM) has become a standard tool in the electromagnetic analysis of electrical machines. Radial-flux machines can often be sufficiently analyzed with the 2-D FE method (Chari and Silvester 1971, Arkkio 1987), while 3-D formulations are needed

to analyze, for instance, the end regions of radial-flux machines (Weiss and Stephens 1981, Lin 2010, Stermecki et al. 2012) or machine constructions which cannot be reasonably simplified to 2-D domains, e.g. axial-flux machines (Li et al. 2011).

The following discussion on the theory and modeling approaches for the core and stray-load losses has been divided into two parts, the first focusing on grid-supplied synchronous machines and the second on additional inverter losses. The iron-loss models will be discussed in more details in the next section.

2.1.1 Losses in Grid-Supplied Synchronous Machines

The stray-load losses of synchronous generators were experimentally studied already by Brainard (1913), and an extensive qualitative investigation of their causes was presented by Richardson (1945). Pole-face losses have been a topic of intensive research, e.g., by Spooner and Kinnard (1924), Gibbs (1947), Aston and Rao (1953), Carter (1955), and Greig and Mukherji (1957). Karmaker (1982) analytically estimated the tooth-ripple losses on the surface of a laminated synchronous-machine rotor. In 1992, he performed comprehensive loss measurements for a 750-hp (560-kW) salient-pole synchronous machine. The losses in the stator end plates, in the laminations close to the end plates and the ventilation ducts, and on the rotor surface were measured. The losses were also sufficiently estimated by analytical methods.

Owing to their computational efficiency, analytical methods have maintained their popularity in the everyday design of synchronous generators and DOL motors up to the present. Traxler-Samek et al. (2008) combined separate analytical models for power losses, air flow, and temperature calculation into one coupled algorithm to allow the simultaneous optimization of both the electromagnetic and thermal performance of a hydrogenerator. The model was applied to determine local hot spots in the stator winding (Traxler-Samek, Zickermann and Schwery 2010). The same group also developed detailed analytical calculation tools for both stator iron losses (Traxler-Samek and Ardley 2009) and damper-winding losses (Traxler-Samek, Lugand and Schwery 2010). The approaches were based on analytical solution of the flux-density distributions in the stator yoke and the air gap.

Numerical tools are used for more challenging design tasks. Karmaker and Knight (2005) used a combination of magnetostatic FE analysis and

an analytical calculation method to model the effect of stator slot skewing on the performance of a large hydrogenerator. They were able to predict the harmonic damper-winding currents sufficiently well. In addition, an interesting study on the pole-face losses showed an increase of 18 % as a result of the skewing of the stator slots. Computationally efficient static FEM was also utilized by Knight et al. (2009 a,b), who derived the pole-face losses, stator core losses, and damper currents analytically from a few 2-D FE solutions. They found the inter-bar losses, the air-gap flux-density induced pole-face losses, the stator core losses, and the damper-winding losses to be extremely sensitive to the bar-to-iron contact resistance in a skewed machine. Englebretson (2009) reached the same conclusion for the inter-bar currents in a skewed-rotor induction machine.

Schmidt et al. (2005) studied the losses in the stator clamping systems of large hydrogenerators by means of 3-D FEM. Both Liu et al. (2011) and Merkhouf et al. (2011) applied the dynamic core-loss model of Lin et al. (2004) and evaluated the performance of a high-speed wound-rotor synchronous motor and a large hydrogenerator, respectively, by applying 2-D FEM.

2.1.2 Additional Inverter Losses

The additional losses and temperature rises caused in electrical machines by the non-sinusoidal voltage waveform of frequency converters have been studied intensively over the last couple of decades. Several interesting studies on the additional inverter losses can be found, but most of these seem to focus on induction machines. For instance, Knight and Zhan (2008) estimated the rotor core losses of a cage induction machine by predicting the flux-density harmonics caused by a pulse-width modulated (PWM) voltage supply. Dlala and Arkkio (2009) studied the PWM losses at different supply frequencies, while Itoh and Ogura (2010) estimated the total losses of two drive systems consisting of a PWM inverter and induction and permanent-magnet motors. Aarniovuori et al. (2012) performed a similar study for an induction motor under direct torque control (DTC) with different switching frequencies.

Considering the large number of analytical studies performed 60 years ago to model the pole-face losses in synchronous generators and DOL motors, surprisingly few efforts have been made to include the effect of inverter supply on synchronous-machine models. Laminated poles in particular have not received very much attention in the literature.

Emery and Eugene (2002) briefly mentioned that laminated rotors should not be severely affected by the inverter supply, but kept their main focus on solid pole shoes, which were considered a much more severe case. Losses in solid poles were also studied by Vetter and Reichert (1994), who modeled the damper-winding and rotor-iron currents by means of a lumped circuit model with its parameters determined by FEM. Park et al. (2008) analyzed a solid-rotor synchronous reluctance machine supplied from a PWM inverter using an equivalent circuit model.

The effect of DTC on the losses of solid-rotor synchronous machines was simulated with FEM by Shisha (2008) and Shisha et al. (2012). They made the interesting observation that the additional inverter-induced eddy-current losses occur mostly on the lagging edge of the pole shoe. They noticed a decrease in these time-harmonic losses with increasing pole-plate conductivity, contrary to the behavior of the losses induced by spatial harmonics. Subsequently, they proposed using specially designed pole shoes with high conductivity on the lagging edge and low conductivity on the leading edge.

Both structural optimization and improved control algorithms have been applied in order to minimize the additional inverter losses. For synchronous machines, Stranges and Dymond (2003) proposed using a large depth-to-width ratio for damper winding slots in order to increase the leakage inductance of the damper bars and to suppress the harmonic contents of the terminal current. Islam (2010) found that the additional eddy-current losses in a form-wound stator winding decreased significantly when the conductors were radially moved further away from the air gap. Zhou and Hu (2008) developed a DTC strategy yielding low harmonic contents on the flux and thus reducing the rotor losses compared to the traditional DTC algorithm. Shisha and Sadarangani (2009) studied a DTC-inverter-fed solid-rotor synchronous machine and noticed a 39 % reduction in the pole-plate losses when zero-voltage vectors were included in the DTC algorithm. A voltage control scheme to minimize the total losses of solid-rotor synchronous machines was implemented by Mademlis et al. (1998, 2000). In addition, LC filters between the inverter and the machine were proposed by Park et al. (2008) and Hatua et al. (2012) to reduce the harmonics in the terminal voltage.

2.2 Iron-Loss Estimation in Finite-Element Analysis

Despite the huge amount of research done over several decades on the fields of numerical electromagnetics and modeling of electrical machines, the prediction of iron losses in the laminated cores has remained a challenge up to this date. Below, different models for iron losses and methods for treating them in FE analysis are reviewed.

2.2.1 Theory and Experimental Models for Iron Losses

Both Steinmetz (1892) and Bertotti (1988) studied the losses in ferromagnetic laminations supplied by a unidirectionally and sinusoidally alternating flux. They found that the losses approximately obey certain power functions of the amplitude of the average flux density \hat{B} and frequency f . Steinmetz separated the losses originating from magnetic hysteresis and eddy currents, and expressed the total losses as

$$P_{\text{Fe}} = \underbrace{c_{\text{hy}} f \hat{B}^{1.6}}_{\text{hysteresis loss}} + \underbrace{c_{\text{cl}} f^2 \hat{B}^2}_{\text{eddy-current loss}}. \quad (2.1)$$

His original formula has undergone several different modifications for better approximations, many of which were summarized by Villar et al. (2008). Bertotti statistically segregated the total iron losses into hysteresis, classical eddy-current, and excess losses with the following frequency and amplitude dependencies:

$$P_{\text{Fe}} = \underbrace{c_{\text{hy}} f \hat{B}^2}_{\text{hysteresis loss}} + \underbrace{c_{\text{cl}} f^2 \hat{B}^2}_{\text{classical loss}} + \underbrace{c_{\text{ex}} f^{1.5} \hat{B}^{1.5}}_{\text{excess loss}}. \quad (2.2)$$

The classical losses were assumed to be caused by the macroscopic eddy currents not affected by the domain structure of the material. On the contrary, the excess losses were explained by the microscopic eddy currents caused by the movement of the domain walls during the magnetization process (Graham 1982). Bertotti's statistical theory has also become widely accepted by many authors. In the models based on this approach, the classical loss is usually calculated analytically for a lamination with a conductivity σ by assuming a uniform flux density over the thickness d , which yields

$$c_{\text{cl}} = \frac{\sigma d^2 \pi^2}{6} \quad (2.3)$$

for the eddy-current loss coefficient (Lammeraner and Štafl 1964). The coefficients c_{hy} , c_{ex} for the hysteresis and excess losses, respectively, are

usually determined experimentally from a set of measurements with different amplitudes and frequencies of sinusoidally alternating flux density (Bertotti 1988, Pluta 2010). However, even if suitable parameters are found to obtain correct losses with sinusoidal excitation, the superposition of the losses given by (2.2) for each harmonic component of non-sinusoidal flux densities may lead to highly erroneous results, as shown, e.g., by Albach et al. (1996). Better extensions for arbitrary waveforms have been presented, e.g., by Fiorillo and Novikov (1990) and Chen et al. (2010).

An obvious sign of the experimental nature of the models based on the statistical loss-segregation theory is that the excess losses, or *anomalous losses*, as they were called earlier, were originally introduced to explain the differences between the measured iron losses and the loss given by the first two terms of (2.2) with the uniformity assumption (2.3) (Overshott et al. 1968). More recently, Mayergoyz and Serpico (1999) stated that the excess loss can be at least partly explained if the non-uniform distributions of the flux density and eddy currents in the lamination thickness are modeled accurately instead of a uniform distribution being assumed. The same had already been discussed by Dupré, Gyselinck and Melkebeek (1998) and was later confirmed by Zirka et al. (2010). This observation means that the contribution of the excess eddy currents to the total iron losses may actually be smaller than predicted by Bertotti's theory, and that the skin effect of the classical eddy currents should be modeled for accurate results.

To avoid the computational burden of accurate skin-effect modeling, Zirka et al. (2006) and Dlala (2008b) used experimentally derived differential equations to increase the phase lag between the field strength and flux density, thus also increasing the eddy-current losses from the value obtained with the low-frequency assumption (2.3). These simplified models seemed to give very good results within certain frequency ranges for the materials for which they were identified. However, the identification for different sheet materials has to be performed by comparison to measurements with several different frequencies, which complicates their use when compared to models with only a few physically meaningful parameters to be identified. Below, a more detailed investigation of physical eddy-current loss modeling is presented.

2.2.2 Physical Eddy-Current Loss Models

Physical models for core lamination eddy currents are based on the solution of the quasistatic Maxwell equations in the electrically conducting domain. Combining Ampere's and Faraday's laws yields

$$\nabla \times \nabla \times \mathbf{H}(x, y, z, t) = -\sigma \frac{\partial \mathbf{B}(x, y, z, t)}{\partial t} \quad (2.4)$$

for the flux density \mathbf{B} and field strength \mathbf{H} . Different 3-D FE approaches for this problem in laminated domains have been presented, for example, by Silva et al. (1995), Preis et al. (2005), Du et al. (2009), and Yamazaki and Fukushima (2010). However, this generally 3-D problem can often be simplified by assuming that the flux-density and field-strength vectors lie in the x-y plane parallel to the lamination, and neglecting the return paths of the eddy currents at the edges (Bottauscio et al. 2000b). With these assumptions, the problem reduces to a 1-D diffusion equation describing the penetration of the flux density into the thickness of the sheet (Del Vecchio 1982):

$$\frac{\partial^2 \mathbf{h}(z, t)}{\partial z^2} = \sigma \frac{\partial \mathbf{b}(z, t)}{\partial t}. \quad (2.5)$$

Here, the 1-D nature of the quantities, i.e., their dependency only on the z coordinate along the thickness, is indicated by the use of lower-case letters.

Both (2.4) and (2.5) have to be coupled with the local $\mathbf{H}(\mathbf{B}(x, y, z, t))$ or $\mathbf{h}(\mathbf{b}(z, t))$ relationship, which, in ferromagnetic materials, is hysteretic but also rate-dependent if the excess eddy currents are taken into account. As the solution, the flux-density distribution in the lamination and its time-dependency are obtained, and can be used to derive the hysteresis, classical eddy-current, and excess losses. Alternatively, the total loss dissipation in the lamination can be determined by integrating the Poynting vector over the surface of the lamination. As shown by Atallah and Howe (1993), the instantaneous power dissipation in the 1-D case is determined by the dynamic relationship between the average flux density and the surface field strength.

The simplest possible solution for (2.5) is obtained if the flux density is assumed to be uniform across the thickness of the lamination ($\mathbf{b}(z, t) = \mathbf{b}_0(t)$), and the constitutive law is required to be satisfied only on the spatial average. In this case, spatial integration of (2.5) yields a parabolic field strength with a surface value of

$$\mathbf{h}_s(t) = \mathbf{h}(\mathbf{b}_0(t)) + \frac{\sigma d^2}{12} \frac{d\mathbf{b}_0(t)}{dt}, \quad (2.6)$$

and the total classical losses with a sinusoidal flux density equal to those calculated using (2.2) and (2.3) (Gyselinck et al. 1999). This model is often called the *classical low-frequency approximation* of the eddy currents.

1-D FE models for the numerical solution of (2.5) have been reported by Bottauscio et al. (2000a), Dlala, Belahcen and Arkkio (2008a), Pippuri (2010), and Yamazaki and Fukushima (2011). Hysteretic material properties were included in the first two models, while the last two assumed single-valued (SV) nonlinearity. The magnetic vector-potential formulation was chosen in all four models.

More recently developed homogenization algorithms provide an alternative to the FE discretization of the lamination. Krah et al. (2002) assumed the flux density to be parabolic in shape and compared such a solution to a finite-difference model. Gyselinck et al. (2006) and Dular (2008) extended the low-frequency approximation (2.6) by expressing the flux density as a series expansion of a finite set of orthogonal polynomial basis functions, weakly expressing the constitutive material law and thus obtaining an equation system for the flux-density coefficients. Results from the homogenized models were found to correspond well to those from FE solutions. However, so far all the homogenization approaches that have been presented have considered only SV materials, and coupling to hysteretic material properties has not yet been reported.

The main difference between the accurate solution of (2.5) and the statistical approach of (2.2) is that the frequency- or amplitude-dependency for the three loss components cannot be explicitly defined, even for sinusoidal flux densities. The constitutive magnetic material law affects the flux-density distribution inside the lamination, causing the eddy-current loss to be dependent on the $\mathbf{h}(\mathbf{b}(z, t))$ relationship, unlike the middle term of (2.2). Similarly, the hysteresis and excess losses depend on the local value of the flux density in the lamination thickness and are thus affected by the skin effect. A detailed investigation of the interdependency of the different loss components was performed by Dlala, Belahcen, Pippuri and Arkkio (2010).

2.2.3 Modeling of Hysteresis and Excess Losses

The highly nonlinear and hysteretic properties of ferromagnetic materials complicate the estimation of iron losses and effectively prevent analytical models from giving accurate results. Numerous different methods for modeling magnetic hysteresis have been presented, the most generally

used approaches within FE analysis being the Jiles-Atherton (JA) model (Jiles and Atherton 1986) and the Preisach model (Mayergoyz 1986). Since the development of new hysteresis models is beyond the scope of this work, an existing vector Preisach model will be used in the analysis and thus the basic concepts required for its implementation and identification are reviewed here. The JA model is also briefly discussed. At the end, models for excess losses are reviewed.

Scalar Hysteresis Models

The JA model is a physical model based on analytical modeling of the behavior of the magnetic domains under an externally imposed magnetic field. Inverted models using the flux density as the input variable have also been presented for more comfortable implementations with vector-potential FE formulations (Sadowski et al. 2002). The main advantage of the JA model is its light computational burden. However, identification of the five required parameters by comparison to experimental data is quite challenging and often requires the use of an optimization algorithm (Lederer et al. 1999, Leite et al. 2003, Cao et al. 2004).

According to Mayergoyz (1986), the idea of the Preisach model was originally proposed by Preisach (1935) and later formulated mathematically by Krasnoselskii and Pokrovskii (1983). The model is based on the mathematical formulation of a simple hysteresis operator $\gamma_{h^+h^-}(h(t))$ characterized by the increasing (h^+) and decreasing (h^-) switching values of the input magnetic field strength $h(t)$, and having a value of ± 1 depending on the current value of $h(t)$. From these simple operators, a continuous distribution weighted with a function $\mu(h^+, h^-)$ is formed to cover all the possible field-strength values. The flux density is obtained as a double integral of this distribution over all the possible combinations of increasing and decreasing field strengths:

$$b_{\text{hy}}(t) = \iint_{h^+ \geq h^-} \mu(h^+, h^-) \gamma_{h^+h^-}(h(t)) dh^+ dh^-. \quad (2.7)$$

Mayergoyz (1986) presented the geometrical interpretation of the Preisach model and simplified its implementation by introducing the Everett function, which allows complete identification of the model using first-order reversal curves (FORCs), as well as calculation of the model output without the double integration of (2.7). The Everett function E is defined as half of the difference between the reversal-point flux density $b(h^+)$ on the ascending branch of the major loop and the flux density $b(h^+, h^-)$ on the descending FORC starting at the aforementioned reversal point. It

was also proven that the value of the Everett function equals a certain definite integral of μ :

$$E(h^+, h^-) = \frac{1}{2} [b(h^+) - b(h^+, h^-)] = \int_{h^-}^{h^+} \int_{h^-}^y \mu(x, y) dx dy. \quad (2.8)$$

With the above relation, it was shown that the value of the double integral in (2.7) can be calculated by summing up the positive and negative contributions of E .

In order to increase the performance of the Preisach model for vector-potential FE formulations, Dlala et al. (2006) numerically inverted the Everett function and obtained an inverted model using the flux density as the input. In the inverted model, the magnetic field strength is obtained by summing the values of the inverted Everett function F at the ascending and descending reversal points b_k^+ and b_k^- for $k = 1, \dots, N_{\text{rev}}$, respectively:

$$h_{\text{hy}}(b) = -h_{\text{sat}} + 2 \sum_{k=1}^{N_{\text{rev}}} [F(b_k^+, b_{k-1}^-) - F(b_k^+, b_k^-)]. \quad (2.9)$$

Here h_{sat} is the saturation field strength, and the first reversal point is assumed to be at negative saturation.

In the numerical implementation, the values of the Everett function are usually calculated by interpolation from a discrete table stored in the memory (Dlala 2011). As an alternative to the Everett function, Guerra and Mota (2007) developed a simple analytical model to calculate the minor loops. The "vertical distance", i.e., the difference in the flux density between a minor loop and one branch of the major loop, was modeled analytically by means of an exponential formula ensuring the closure of the minor loops. Only a single branch of the major loop and one scalar parameter describing the shape of the minor loops were needed to identify the model.

Vector Hysteresis Models

In addition to the scalar hysteresis models, major attempts have also been made to extend the approaches to model the hysteretic behavior of rotational magnetic fields. This is especially necessary in electrical machines, in which the rotating flux causes the local flux-density and field-strength loci to be rotational rather than unidirectionally alternating. Considering the approaches of this thesis, the following discussion focuses on 2-D vector models, although, 3-D models have also been presented.

Bergqvist (1996) derived a simple vector generalization of the original JA model. Leite et al. (2004) extended the inverted scalar JA model of

Sadowski et al. (2002) for vector fields, and applied it to predict the hysteresis losses in the core of a three-phase transformer (Leite et al. 2009).

A more general mathematical model describing the vectorial behavior of hysteresis was formulated by Mayergoyz (1988*b*). He applied the scalar Preisach model in a semicircle in each possible direction and summed up the outputs to form the output flux-density vector. In the numerical implementation, the semicircle was discretized into a finite number of directions. If the vector extension is performed for the inverted scalar model, the field-strength vector is obtained by projecting the flux density \mathbf{b} into directions $\mathbf{u}_{\phi_i} = i\pi/N_\phi$, $i = 1, \dots, N_\phi$, calculating the field strength with the scalar model for these projections and summing up the outputs:

$$\mathbf{h}_{\text{hy}}(\mathbf{b}) = \sum_{i=1}^{N_\phi} h_{\text{hy}}(\mathbf{b} \cdot \mathbf{u}_{\phi_i}) \mathbf{u}_{\phi_i}. \quad (2.10)$$

Mayergoyz' vector extension is physically justifiable and can also be applied with scalar hysteresis models other than Preisach-type ones. The loss-modeling properties of the model were further improved by Adly and Mayergoyz (1993) and Dlala, Belahcen, Fonteyn and Belkasim (2010) who used an additional parameter to remove the phase lag between the circularly rotating flux-density and field-strength vectors at saturation.

The inverted Everett function of the vector Preisach model has to be identified so that it produces the unidirectionally measured Everett function as the output when supplied with an alternating flux density. Mayergoyz (1988*b*) formulated this identification problem as an integral equation, and also solved the resulting problem analytically. Stoleriu et al. (2008) simplified the integration by means of a change of variables, and used the Gauss-Jacobi quadratures to calculate the integral numerically. Mayergoyz (1988*b*) and Stoleriu et al. (2008) also proposed semi-analytical identification procedures for an anisotropic vector model, while Kuczmann (2009) performed the complete identification by means of a numerical approach.

Excess Losses

Because of to the microscopic scale of the excess eddy currents (Graham 1982), they are usually modeled as a part of the magnetic constitutive law, which thus becomes rate-dependent. Mayergoyz (1988*a*) implemented a rate-dependent Preisach model in which the Preisach distribution function was made dependent on the rate of change of the input field. Dupré, Bertotti and Melkebeek (1998) compared the excess losses pre-

dicted by the dynamic Preisach model and Bertotti's statistical loss theory (2.2) and found similar behavior on the part of the excess losses with respect to the frequency.

A dynamic extension of the JA model was presented by Brockmeyer and Schulting (1993). Jiles (1994) also modified the equations of the scalar JA model so that the magnetic energy balance included the contributions of the last two terms of (2.2).

Similarly to the classical low-frequency approximation (2.6) and the approach of Jiles (1994), Righi et al. (2001) defined an excess field-strength term in such a way that the average magnetic power dissipated over one cycle of a sinusoidally alternating average flux density equaled the excess loss given by (2.2):

$$\mathbf{h}_{\text{ex}}(t) = c_{\text{ex}} \left| \frac{d\mathbf{b}_0(t)}{dt} \right|^{-0.5} \frac{d\mathbf{b}_0(t)}{dt}. \quad (2.11)$$

This excess term was added to the field strength obtained from a static vector hysteresis model to obtain a rate-dependent constitutive law.

The excess-loss coefficient is often presented as $c_{\text{ex}} = \sqrt{\sigma G V_0 S}$, with the parameters G , V_0 , and S related to the properties of the lamination as explained by Bertotti (1985, 1988). $G \approx 0.1356$ is a constant describing the damping effect of the local excess eddy currents around a domain wall. V_0 is a characteristic field strength determining the ability of an external field to increase the number of simultaneously active magnetic objects, i.e., groups of interacting domain walls. S is the cross-sectional area of the lamination, the use of which causes the excess losses to actually be geometry-dependent rather than local in nature.

2.2.4 Loss Models in Finite-Element Analysis

Commonly Used Loss Models

Most FE tools treat laminated magnetic cores as lossless regions during the computation, and calculate the losses only at the post-processing stage from the solved flux-density distribution. Many recently published works on the estimation of iron losses (e.g., Huang et al. 2012, Hargreaves et al. 2011) still rely on experimental formulas more or less similar to (2.1) or (2.2), which are easy to implement and can often be identified by the data given by the manufacturer of the core laminations.

Gyselinck et al. (1999) included the classical low-frequency eddy currents (2.6) into a 2-D FE model of electrical machines by adding the rate-

dependent term to the SV reluctivity. In (Gyselinck et al. 2000), a vector Preisach model was also included. The same model was also applied by Knight et al. (2011) to study eddy-current losses with PWM supply. Righi et al. (2001) took into account the inverted JA model and the excess field-strength term of (2.11). It was concluded that only minor changes to traditional lossless 2-D FE formulations are needed to account for these effects.

Bottauscio et al. (2000*a*, 2002) were the first to couple a FE solution of (2.5) to a 2-D FE model. The coupling was implemented in a local manner by solving the diffusion equation at each integration point of the 2-D geometry, thus replacing the magnetic constitutive law by the dynamic relationship between the surface field strength and the average flux density. In the first paper (2000*a*), the coupling was implemented as a nested iteration procedure by solving the diffusion equation separately at each 2-D integration point while forming the system matrix. In the latter paper, the 2-D and 1-D equations were implemented as a single coupled system of equations. The nested iteration approach was also taken later by Dlala, Belahcen and Arkkio (2008*a*) and Pippuri (2010), who included the iron losses in complete 2-D FE models of induction machines. Yamazaki and Fukushima (2011) only used their model in the post-processing stage, but performed an interesting comparison of the results to a full 3-D FE model for the eddy currents. The 2-D/1-D approach proved to estimate the iron losses in induction and permanent-magnet machines almost equally to the 3-D model.

As already mentioned, homogenization methods have started to gain increasing attention in addition to finely discretized FE models for the eddy-current problem. Their development is mostly driven by the need for 3-D computation, in which fine discretization of lamination stacks would result to unacceptably large systems of equations. Dular et al. (2003) modeled a 3-D lamination stack as a continuum in which the eddy currents were treated analytically in the frequency domain. The linear and non-linear time-domain extensions (Gyselinck and Dular 2004, Gyselinck et al. 2006, Dular 2008) were applied in a 3-D FE model of a laminated-core toroid. The same method was recently applied in a globally coupled 2-D vector-potential formulation and used to analyze a switched reluctance motor (Gyselinck et al. 2011). Somewhat similar homogenization approaches have also been developed to treat eddy currents in windings (Sabariago et al. 2008).

Although many attempts have been made to include the iron losses in the FE formulations, not many published works are available to assess the effect of the losses on the FE solution. Dupré, Gyselinck and Melkebeek (1998) compared the flux patterns in a transformer T-joint calculated with FE formulations including both SV materials and a vector Preisach model in the solution. A clear difference could be seen in the flux distributions, but the difference between the losses was not stated. Dlala, Belahcen and Arkkio (2010) performed a more detailed study on the effect of iron losses on the field solution of induction machines. They found the total iron losses to be reduced by up to 15 % after the inclusion of the losses in the FE formulation. This was stated to be caused by the damping effect of the iron losses on the inducing field. The mechanical and electrical quantities were found to be almost unaffected.

Implementation Practices

In the traditional FE formulations in magnetics, e.g. Chari and Silvester (1971), Arkkio (1987), the discrete equation system has been expressed as the product of the stiffness matrix and the vector of unknowns. The apparent problem arising from the hysteretic materials is that the magnetic reluctivity can have any value between negative and positive infinity, and thus the stiffness matrix does not have a physical meaning. Two main approaches have been used to overcome this problem and to include the hysteretic nonlinearity into vector-potential FE formulations: the differential reluctivity (DR) tensor and the fixed-point (FP) iteration.

The use of the DR tensor is based on the assumption that the derivative of the field strength with respect to the flux density is always positive (or positive definite for vector fields). Righi et al. formulated the 2-D FE equations by using the DR tensor to solve the increase in the vector potential per time step instead of the actual value. They first considered SV materials (2000) and later hysteretic ones (2001). The nonlinear equation system was solved with the method of successive iterations. Another possibility is to spatially discretize the weak form of Ampere's law without segregating the stiffness matrix, and to apply the DR tensor in the iteration with, for example, the NR method (Gyselinck et al. 2004).

In the FP method, the stiffness matrix is formed assuming a constant reluctivity and the nonlinearity is taken into account as a residual error from the previous iteration. This method has been used quite widely in different formulations (Chiampi et al. 1980, 1995, Bottauscio et al. 1995,

Dlala and Arkkio 2007, Mathekga et al. 2011). The FP method is typically stable but converges slowly. Dlala, Belahcen and Arkkio (2008b) accelerated the convergence by calculating the DR tensor and updating the FP reluctivity once per time step for each local integration point.

2.3 Calorimetric Measurement of Losses

2.3.1 Calorimetric Methods

Theoretically, the power losses of an electrical machine are obtained as the difference between the input and output powers of the machine. However, owing to the relatively high efficiency of electrical machinery, this input-output method may lead to unacceptably inaccurate results even with small measurement errors in the input and output powers (Lindström 1994, Bradley et al. 2006). Standard IEC/EN 60034-2:2007 gives maximum limits for the measurement errors related to the power measurements, but these may be difficult to achieve, especially if the machine under test is supplied from an inverter.

Calorimetric measurement systems, regulated, e.g., by the standard IEC/EN 60034-2a:1974, are used to determine the power losses from the heat dissipation of the machine. If the part of the input energy converted into sound is neglected, the heat dissipation equals the loss of the machine, and the problem of loss measurement is reduced to measurement of the heating power. Numerous calorimetric measurement systems have been reported during the course of the last 20 years, most of these designed for induction machines up to the power range of a few tens of kilowatts. The highest-power calorimeter reported so far seems to be the one designed by Cao, Huang and French (2009) for a 300-kW induction machine. The most common calorimeter constructions were classified by Cao, Asher, Huang, Zhang, French, Zhang and Short (2010) into four different types: the direct gas-cooled open-cycle-type, the direct liquid-cooled closed-cycle-type, the indirect balanced-type and the indirect series-type calorimeters.

In the direct calorimeters, the power loss is determined directly by measuring the rate of change of the coolant's thermal energy. The coolant can be either gas or liquid. Especially with gas coolants, however, accurate measurement of the specific heat capacity and the temperature dis-

tribution across the coolant ducts may be difficult (Turner et al. 1991, Cao, Asher, Huang, Zhang, French, Zhang and Short 2010). In addition, the heat leakage also has to be accurately measured or minimized so as to be negligible. To overcome these problems, Cao, Bradley and Ferrah (2009) developed a direct air-cooled high-precision calorimeter trying to minimize both the heat leakage and the variations in the air properties. They reported an accuracy of ± 5.6 W, i.e. $\pm 0.12\%$ in the loss range of 0...4.5 kW. Water-cooled, closed-cycle systems were reported by Szabados and Mihalcea (2002) and Weier et al. (2006). The former system was designed for a 7.5-kW induction motor, but the overall accuracy of the system was not stated. The latter was designed for power-electronic equipment with losses up to 20 W. An accuracy of ± 0.4 W, i.e. $\pm 2\%$, was reported.

To eliminate the effects of the variations in the air properties and temperature, balance calorimeters are commonly used. In the balance method, the calorimeter is calibrated against a known heat source (IEC/EN 60034-2A 1974), usually a heater resistor. Turner et al. (1991) developed a balance calorimeter for the measurement of a 5.5-kW induction motor. They obtained measurement errors of 1.45 % and 4.7 % for the total electromagnetic losses in full-load and no-load operation, respectively. Lindström (1994) built an air-cooled balance calorimeter for a small induction machine. However, his error estimates relied on seemingly uncertain assumptions about the temperature distributions inside the calorimeter.

The major drawback of the balance method is that for accurate results, the calibration test should be performed after each actual test run. This significantly increases the measurement time, but also makes the system sensitive to the variations in the air properties during the course of the measurement. Zhang et al. (2011) suggested using a precalculated calibration curve to eliminate the need for calibrating after each test run. However, they emphasized the need for frequent calibration of the system.

In double-chamber or series-type calorimeters, the calibration measurements are performed simultaneously with the actual test run. The same coolant gas is run through two separate chambers, the first one containing the test machine and the second one the calibration heater. Since the coolant properties remain similar in the two chambers, the power losses in the test machine can be determined by measuring the heater power and comparing the temperature rises of the coolant in both chambers. Such

calorimeters were implemented by Jalilian et al. (1999), Mei et al. (2001) and Sun et al. (2012). Using the double-chamber calorimeter shortens the measurement time when compared to the balance test but complicates the system construction. In addition, some uncertainty is obviously caused by heat-leakage differences due to higher coolant temperature in the latter chamber.

2.3.2 Specific Applications

Owing to their good accuracy, the calorimetric methods can be used to measure differences in losses between machines with different structural constructions or different supply-voltage waveforms. However, the published work on calorimetric systems has generally been more focused on the design and implementation considerations, and specific applications have been presented only by relatively few research groups.

Turner et al. (1991) evaluated the effect of air-gap length on the losses of the 5.5-kW induction motor. Jalilian et al. (1999) briefly mentioned the applicability of their double-chamber calorimeter for accurate measurement of differences in losses between machines with distorted and purely sinusoidal voltage supplies. Knight et al. (2005) used a water-cooled double-jacketed calorimeter to determine the effect of loading and modulation technique on the total losses of a 375-W skewed-rotor induction motor. The same setup was also used by Wu et al. (2006) and Zhan et al. (2008) to study the effect of different PWM schemes on the motor losses, and to verify FE simulation results. Later, in (Wu et al. 2008, 2011), the inverter losses were also measured.

Few interesting papers have been published on the evaluation of the loss-measurement and segregation methods proposed by different standards using the calorimetric method. Bradley et al. (2006) applied their high-precision calorimeter to determine the stray-load losses of induction machines. They compared the results of the calorimetric method to the input-output methods suggested by several induction motor testing standards, and thoroughly analyzed the sources of error in the stray-load losses determined by loss segregation. Cao (2009) performed a careful comparison of the differences in the stray-load loss and efficiency estimations of IEEE Std 112-2004 and IEC/EN 60034-2:2007, and used the calorimeter as a reference to evaluate the accuracy of the approaches suggested by each standard. In (Cao, Bradley, Clare and Wheeler 2010), the authors determined the stray-load losses and additional inverter losses of

induction motors with powers ranging from 1.1 to 30 kW.

Recently, improved design procedures have been suggested for the calorimetric systems. Zhang et al. (2010) used computational fluid dynamics (CFD) calculations in the design of a calorimeter for induction machines up to 30 kW. They emphasized the importance of accurate knowledge of the fluid flows inside the calorimeter in order to reduce heat leakage and the temperature gradients in the inlet and outlet ducts. Later, in (Zhang et al. 2011), they analyzed an existing balance calorimeter with the same CFD approach.

2.4 Summary and Conclusions

In the above study, the origin of and modeling approaches for core and stray-load losses, several methods for iron-loss modeling and calorimetric measurement systems were reviewed. It can be concluded that the additional inverter losses in laminated-core synchronous machines have not been studied very much before, which is slightly surprising considering the use of thick steel sheets in the rotor poles. It is also clear that accurate iron-loss modeling and, especially, the inclusion of the iron losses into the 2-D FE analysis of electrical machines is still far from being everyday routine. Most of the existing approaches only consider the iron losses as a local phenomenon and globally coupled models had not been presented until the paper of Gyselinck et al. (2011). Another issue discussed very little so far is the effect of the iron losses on the field solution.

The 2-D FE model with eddy-current losses developed during this work will be based on the approaches of Gyselinck et al. (2006) and Dular (2008). The static vector hysteresis model and the excess losses will be modeled with the vector Preisach model of Dlala (2008a), and the excess-loss model of Righi et al. (2001). A simple semi-analytical identification process for the inverted Everett function based on the approaches of Guerra and Mota (2007) and Stoleriu et al. (2008) will be attempted. The coupling of the iron losses to the 2-D FE model will be performed in a global manner in order to achieve good computational performance. The model will be applied to study the effect of the inclusion of the iron losses on the FE solution of wound-field synchronous machines.

Several different calorimetric measurement systems have been proposed by other researchers, most of these being designed for induction machines. Considering that one aim of this work is to study the effect of the rotor

lamination material on the total core losses of synchronous machines, the calorimetric measurements can be seen as the only reasonable method of measurement if sufficient accuracy is to be obtained. An air-cooled open-cycle calorimeter will be implemented and the balance method will be applied to obtain accurate results. The size of the test machine, 150 kVA, seems to be higher than in most of the works presented so far, which have mainly considered devices up to a few tens of kilowatts. In order to estimate the accuracy of the measurement system, a thorough theoretical error analysis will be performed and the differences in the leakage conditions between the balance test and the test run will be estimated.

3. Methods

This chapter presents the methods used for the numerical analysis and the experimental determination of the core losses. In the first two sections, the iron-loss model developed during this work and its FE implementation are presented. In the last section, the calorimetric system built for the experimental determination of the losses is described. The model and the calorimeter have already been presented in Publications II and III, respectively. Thus only the main parts and some specific details missing from the papers are summarized here.

3.1 Iron-Loss Model

This thesis aims for accurate physical modeling of the iron losses on both the stator and the rotor sides of frequency-converter-supplied synchronous machines. Thus neither the statistical approach to the loss modeling nor any of the other experimental models discussed in the previous chapter were considered suitable for the purpose of this work. In addition, especially for the thick rotor sheets to be correctly modeled, it was concluded that the skin effect of the lamination eddy currents has to be considered and that the low-frequency approach (2.3) is not enough. Thus the iron-loss model developed during this work comprises a numerical solution for the flux-density distribution in the thickness of the core lamination and the constitutive material law consisting of models for the magnetic hysteresis and the excess losses. Below, these models are briefly described.

3.1.1 Eddy Currents

The model for lamination eddy currents implemented during this work and presented in Publication II is based on the homogenization approach suggested by Gyselinck et al. (2006) and Dular (2008). This method was

chosen since it does not need FE discretization in the thickness of the lamination, provides the solution directly for the flux density instead of the vector potential, and thus also enables a relatively straightforward global coupling to a 2-D FE model of an electrical machine. In the model, a solution for the diffusion equation (2.5) is sought as a series expansion of the flux density using an orthogonal function space with basis functions $\alpha_n(z), n = 0, \dots, N_b - 1$:

$$\mathbf{b}(z, t) = \sum_{n=0}^{N_b-1} \mathbf{b}_n(t) \alpha_n(z). \quad (3.1)$$

Gyselincx and Dular suggested either polynomial or hyperbolic basis functions. In this work, however, the Fourier series was considered to be the most natural choice (Publication II). Because of the symmetry with respect to the middle point of the lamination thickness, a cosine series can be used:

$$\alpha_n(z) = \cos\left(2n\pi \frac{z}{d}\right). \quad (3.2)$$

To fulfill (2.5) identically, the field strength is expanded as

$$\mathbf{h}_{\text{appr}}(z, t) = \mathbf{h}_s(t) - \sigma d^2 \sum_{n=0}^{N_b-1} \frac{\partial \mathbf{b}_n(t)}{\partial t} \beta_n(z), \quad (3.3)$$

where $\mathbf{h}_s(t)$ is the field strength on the lamination surface and the functions $\beta_n(z)$ are defined in such a way that $\beta_n(\pm d/2) = 0$ and

$$\alpha_n(z) = -d^2 \frac{\partial^2 \beta_n(z)}{\partial z^2}. \quad (3.4)$$

With a finite number of terms in the series expansion, \mathbf{h}_{appr} does not satisfy the constitutive material law $\mathbf{h}(\mathbf{b})$ which is therefore expressed weakly with respect to the basis functions as

$$\frac{1}{d} \int_{-d/2}^{d/2} (\mathbf{h}_{\text{appr}}(z, t) - \mathbf{h}(\mathbf{b}(z, t))) \alpha_n(z) dz = \mathbf{0}, \text{ for } n = 0, \dots, N_b - 1. \quad (3.5)$$

Substituting (3.3) and solving the surface field strength yields the following system of equations describing the behavior of the field in the lamination:

$$\begin{bmatrix} \mathbf{h}_s(t) \\ 0 \\ \vdots \end{bmatrix} = \frac{1}{d} \int_{-d/2}^{d/2} \mathbf{h}(\mathbf{b}(z, t)) \begin{bmatrix} \alpha_0(z) \\ \alpha_1(z) \\ \vdots \end{bmatrix} dz + \sigma d^2 \mathbf{C} \frac{\partial}{\partial t} \begin{bmatrix} \mathbf{b}_0(t) \\ \mathbf{b}_1(t) \\ \vdots \end{bmatrix}. \quad (3.6)$$

The elements of matrix \mathbf{C} are obtained by integration over the lamination thickness as

$$C_{mn} = \frac{1}{d} \int_{-d/2}^{d/2} \alpha_m(z) \beta_n(z) dz, \text{ for } m, n = 0, \dots, N_b - 1, \quad (3.7)$$

which yields

$$C_{mn} = \begin{cases} 1/12, & \text{if } m = n = 0 \\ \frac{1}{2\pi^2(m+n)^2}, & \text{if } m = n > 0 \\ \frac{(-1)^{m+n+1}}{4\pi^2(m+n)^2}, & \text{if } mn = 0 \text{ and } m + n > 0 \\ 0, & \text{otherwise} \end{cases} \quad (3.8)$$

for the cosine terms. The matrix indices are started from zero in order to correspond to the indices of the basis functions.

3.1.2 Constitutive Material Law

In ferromagnetic materials the local $\mathbf{h}(\mathbf{b}(z, t))$ relationship is hysteretic. If the local excess eddy currents are also considered, the total field strength locally in the lamination is obtained as the sum of the hysteretic and excess terms:

$$\mathbf{h}(\mathbf{b}(z, t)) = \mathbf{h}_{\text{hy}}(\mathbf{b}(z, t)) + \mathbf{h}_{\text{ex}}(\mathbf{b}(z, t)). \quad (3.9)$$

In this work, hysteresis is modeled by the existing inverted vector Preisach model developed by Dlala et al. (2006) and Dlala, Belachen and Arkkio (2008). Although the Preisach model is mathematical rather than physical in nature, it is preferred in this work because of its ability to model the minor hysteresis loops. The Preisach model would, in principle, need more measurement data for its identification than, for example, the JA model, but the identification process has been simplified here so that only the static major hysteresis loops are measured and the FORCs are determined analytically, as will be shown in the next subsection. The model has been implemented according to (2.9) and (2.10).

The excess eddy currents were modeled following the work of Righi et al. (2001) by defining an excess field strength according to (2.11). The excess-loss coefficient $\sqrt{\sigma G V_0 S}$ is here considered to be a single material-dependent parameter to be identified from measurements, and the model is applied locally on $\mathbf{b}(z, t)$ independently of the geometry. This is considered justified because of the accurate modeling of the skin effect.

In some of the simulations in this work, SV material properties are assumed instead of hysteretic ones in order to simplify the computation. In this case, the hysteretic material relationship $\mathbf{h}_{\text{hy}}(\mathbf{b})$ is replaced by a SV reluctivity ν :

$$\mathbf{h}_{\text{sv}}(\mathbf{b}) = \nu(|\mathbf{b}|)\mathbf{b}. \quad (3.10)$$

3.1.3 Model Identification

Measurement of Material Properties

In Publication II, identification of the iron-loss model for the induction-machine simulation was performed by means of comparison to unidirectional measurements performed with a single-sheet tester (Fonteyn and Belahcen 2008). The static hysteresis loop was measured at a 5-Hz supply, and the FORCs needed for the calculation of the Everett function were constructed following the numerical approach of Dlala (2011). In addition, the unknown electrical conductivity and the excess-loss coefficient for the sheet were determined by least-squares fitting to 20-Hz, 100-Hz and 500-Hz measurements with different amplitudes.

As discussed in Publication VI and Chapter 4, a synchronous machine equipped with three rotors stacked of different lamination materials was used for the verification of the models used in this work. Performing separate dynamic identification measurements for each material would have required quite a large number of experiments. On the other hand, the availability of three different materials was seen as a good chance to evaluate the performance of the model with the parameters identified from simpler measurements. Thus only the electrical conductivities and the static major hysteresis loops were measured for these three materials, and the rest of the unknowns in the model were estimated by means of analytical methods. The measurements were outsourced to a research center specializing in the measurement of material properties. The samples were 300 mm x 30 mm Epstein strips cut in arbitrary directions to eliminate any effect of anisotropy. The static major hysteresis loops were measured using the REMAGRAPH[®] C - 500 measurement system (Magnet-Physik 2008).

As seen in Publication II, the excess losses were small compared to the other loss components. Segregation of the excess losses from the classical eddy-current losses is extremely challenging and would require comprehensive and accurate dynamic measurements. Thus it was seen as justified to calculate the excess-loss coefficients $\sqrt{\sigma G V_0 S}$ for the three materials by scaling the value obtained in Publication II by the square roots of the conductivities.

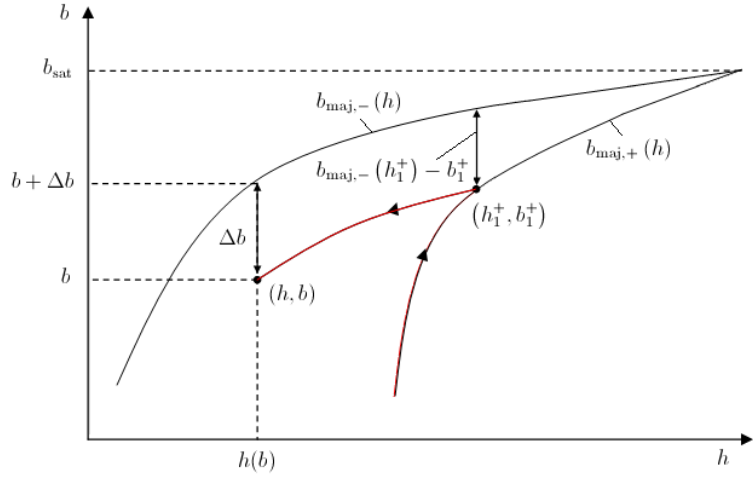


Figure 3.1. Notation in the analytical definition of the FORCs.

Everett Function for the Hysteresis Model

The inverted Everett function needed for the hysteresis model (2.9), had to be estimated on the basis of the measured major loops. Since the numerical approach of Dlala (2011) used in Publication II was found quite slow, and the analytical model for the major loops proved not to be accurate enough, a modified version of the approach of Guerra and Mota (2007) was used instead. The notation used below is given in Figure 3.1. The descending branch of the major loop is defined by the h - and b -based functions $b_{\text{maj},-}(h)$ and $h_{\text{maj},-}(b)$, respectively. The distance along the b -axis between the major loop and a descending FORC is defined analytically as

$$\Delta b(b) = (b_{\text{maj},-}(h_1^+) - b_1^+) \left(\frac{b + b_{\text{sat}}}{b_1^+ + b_{\text{sat}}} \right)^{1+\beta \frac{|b|}{b_{\text{sat}}}}, \quad (3.11)$$

where b_{sat} is the chosen maximum flux density at which the ascending and descending branches of the major loop meet and above which only SV magnetization properties are assumed. β is a constant parameter defining the shape of the FORCs. After Δb is known, the field-strength value can be determined from the major loop as

$$h(b) = h_{\text{maj},-}(b + \Delta b(b)). \quad (3.12)$$

To ensure good accuracy, the analytical function describing the major loop $h_{\text{maj},-}(b)$ suggested by Guerra and Mota (2007) was replaced by direct interpolation from the measured major-loop data. Parameters β were adjusted manually so that the FORCs appeared physically reasonable and did not cross the major loops. For more formal identification of the parameters, FORC measurements would have been needed.

From the FORCs, the Everett function was constructed using (2.8). The identification problem of the vector hysteresis model was solved by the Gauss-Jacobi intergration presented by Stoleriu et al. (2008). The results of the identification are given in Chapter 4 and Publication VI.

3.2 Electrical Machine Model

The numerical computations of this work were performed using the 2-D FE software FCSMEK developed in the Department of Electrical Engineering at Aalto University School of Electrical Engineering. The program solves Ampere's circuital law in the 2-D cross section of radial-flux electrical machines by the magnetic vector-potential formulation and nodal polynomial shape functions of either the 1st, 2nd, or 3rd order (Arkkio 1987). Magnetostatic, time-harmonic or time-stepping simulations can be performed, and either current or voltage sources can be used for the windings.

The iron-loss model presented in the previous section was implemented in the time-stepping solver. However, the initial state for the time-stepping simulations of synchronous machines is calculated by the static solver. In the following, the computation of the initial state is first described. Later, details on the FE implementation of the iron-loss model are given.

3.2.1 Initial State for Time-Stepping Simulations

The core losses are analyzed numerically by time-stepping FE analysis. Usually, the losses are to be calculated at a predefined operating point. To minimize the required computation time, the initial state for the time-stepping simulation should be defined in such a way that the desired operating point can be reached in as few supply periods as possible. In this work, a static FE solver combined with a two-axis synchronous-machine model is used to compute the initial state for the time-stepping simulations.

In the static FE solution, nonlinear single-valued reluctivity ν is assumed for the iron. The rotor is set to a given angle α_r , and the cross section Ω is discretized into elements with nodal shape functions $N_i, i = 1, \dots, N$. If the field winding is supplied from a voltage source u_f , the field current i_f is calculated assuming a purely resistive circuit, i.e., synchronous rotation speed. The terminal voltage is assumed to vary sinu-

soidally with an angular frequency ω , and the voltage space vector is divided into the d- and q-axes components $u_{s,d}$ and $u_{s,q}$. The full equation system for a three-phase machine, from which the nodal values $\mathbf{a} = (a_1, a_2, \dots, a_N)$ of the vector potential and the current components $i_{s,d}$ and $i_{s,q}$ are solved, can be written as

$$\begin{bmatrix} \mathbf{S}(\mathbf{a}) & \mathbf{K}_d & \mathbf{K}_q & \mathbf{K}_f \\ \frac{2}{3}N_{\text{sec}}l\omega(\mathbf{K}_d)^T & R_s & \omega L_{s,ew} & \mathbf{0} \\ \frac{2}{3}N_{\text{sec}}l\omega(\mathbf{K}_q)^T & \omega L_{s,ew} & R_s & \mathbf{0} \\ \mathbf{0} & \mathbf{0} & \mathbf{0} & R_f \end{bmatrix} \begin{bmatrix} \mathbf{a} \\ i_{s,d} \\ i_{s,q} \\ i_f \end{bmatrix} = \begin{bmatrix} \mathbf{0} \\ u_{s,d} \\ u_{s,q} \\ u_f \end{bmatrix}. \quad (3.13)$$

The elements of the magnetic stiffness matrix resulting from the spatial discretization of the weak form of Ampere's law are obtained as

$$S_{ij}(\mathbf{a}) = \int_{\Omega} \nu(\mathbf{a}) (\nabla N_i) \cdot (\nabla N_j) d\Omega, \quad (3.14)$$

the vectors \mathbf{K}_d , \mathbf{K}_q and \mathbf{K}_f describe the d- and q-axis armature-winding flux linkages and the field-winding flux linkage, respectively. R_s , R_f and $L_{s,ew}$ are the stator and field windings resistances and the stator end-winding inductance, respectively. In the voltage equations, the factor $2/3$ results from the space-vector theory for a three-phase machine, N_{sec} is the number of modeled symmetry sectors in the whole cross section, and l is the core length. After the solution, the torque and the electrical powers are calculated according to the two-axis theory.

Since many different loading conditions were to be analyzed during this work, an automatic procedure was needed to force the steady-state solution into the desired operation point. This means that the rotor angle α_r and the field voltage u_f have to be adjusted in such a way that the desired active power P_{ref} and reactive power Q_{ref} are obtained. The two powers $P(u_f, \alpha_r)$ and $Q(u_f, \alpha_r)$ can be considered to be dependent on the rotor angle and field voltage by unknown nonlinear functions representing the FE solution. Thus the problem has to be solved iteratively, starting from certain initial values. If the NR method is applied, the residual vector and the Jacobian matrix for the problem, respectively, read

$$\mathbf{r} = \begin{bmatrix} P(u_f, \alpha_r) \\ Q(u_f, \alpha_r) \end{bmatrix} - \begin{bmatrix} P_{\text{ref}} \\ Q_{\text{ref}} \end{bmatrix} \quad (3.15)$$

$$\mathbf{J} = \begin{bmatrix} \frac{\partial P(u_f, \alpha_r)}{\partial u_f} & \frac{\partial P(u_f, \alpha_r)}{\partial \alpha_r} \\ \frac{\partial Q(u_f, \alpha_r)}{\partial u_f} & \frac{\partial Q(u_f, \alpha_r)}{\partial \alpha_r} \end{bmatrix}. \quad (3.16)$$

The Jacobian matrix cannot be calculated analytically and is thus approximated numerically at each iteration step after the solution of the

residual. This is done by imposing small differences, e.g., $\Delta u_f = 0.01$ V and $\Delta \alpha_r = 0.01^\circ$, on the voltage and the angle in turn, solving the system again, and approximating the partial derivatives numerically from the differences in the solutions:

$$\mathbf{J} \approx \begin{bmatrix} \frac{P(u_f + \Delta u_f, \alpha_r) - P(u_f, \alpha_r)}{\Delta u_f} & \frac{P(u_f, \alpha_r + \Delta \alpha_r) - P(u_f, \alpha_r)}{\Delta \alpha_r} \\ \frac{Q(u_f + \Delta u_f, \alpha_r) - Q(u_f, \alpha_r)}{\Delta u_f} & \frac{Q(u_f, \alpha_r + \Delta \alpha_r) - Q(u_f, \alpha_r)}{\Delta \alpha_r} \end{bmatrix}. \quad (3.17)$$

If the NR iteration diverges, it can be started over from a different initial angle until convergence is reached.

The initial state obtained from the static solution does not take into account the iron losses, the damper-winding currents or any harmonic contents in the flux. However, it is computationally efficient and provides a starting point reasonably close to the steady state of the time-stepping simulation. Indeed, according to experiments, the latter of two subsequent simulation periods with zero-slip operation is usually close enough to the steady state to provide a good estimate of the losses.

3.2.2 Finite-Element Implementation of the Iron-Loss Model

To estimate the core losses of a whole synchronous machine, the developed iron-loss model needed to be coupled to the 2-D FE model of an electrical machine. According to the literature review, the most common way of implementing such loss models within FE analysis tools is to use the lamination model locally at each 2-D integration point. This is the natural choice for post-processing models but problems may arise if the iron losses are to be coupled to the 2-D field solution. First of all, convergence problems may arise if the two models are solved with two nested iteration procedures (Pippuri 2010). Secondly, especially with 2nd- or higher-order FEs in the 2-D model, the number of integration points is usually high when compared to the number of nodes, and thus the computational burden easily becomes high. Keeping these problems in mind, a globally coupled approach was attempted in this work in order to obtain better convergence and better computational performance.

In the time-stepping 2-D FE analysis the iron-loss effects are included in the field solution by applying Ampere's law to the surface field strength (3.6) in the laminated regions of the cross section. Since the tangential component of the field strength is continuous over material boundaries, and no currents are present between adjacent laminations, the source

term becomes zero:

$$\nabla_{\mathbf{xy}} \times \mathbf{H}_s(x, y, t) = \left(\frac{\partial H_{s,y}(x, y, t)}{\partial x} - \frac{\partial H_{s,x}(x, y, t)}{\partial y} \right) \mathbf{u}_z = \mathbf{0}. \quad (3.18)$$

Capital letters are used in the 2-D model to denote the x - y dependency, and the del operator is written as $\nabla_{\mathbf{xy}}$ to emphasize that it is operating only in the x - y plane. To keep the final equation system symmetric, the curl is applied to all the equations of system (3.6). To fulfill Gauss' law for magnetics, the flux-density components $\mathbf{B}_n, n = 0, \dots, N_b - 1$ are expressed as curls of the corresponding vector-potential components. The total system of equations in the laminated regions thus becomes:

$$\mathbf{B}_n(x, y, t) = \nabla_{\mathbf{xy}} \times \mathbf{A}_n(x, y, t), \text{ for } n = 0, \dots, N_b - 1 \quad (3.19)$$

$$\mathbf{B}(x, y, z, t) = \sum_{n=0}^{N_b-1} \mathbf{B}_n(x, y, t) \alpha_n(z) \quad (3.20)$$

$$\begin{aligned} \frac{1}{d} \nabla_{\mathbf{xy}} \times \int_{-d/2}^{d/2} \mathbf{H}(\mathbf{B}(x, y, z, t)) \begin{bmatrix} \alpha_0(z) \\ \alpha_1(z) \\ \vdots \end{bmatrix} dz \dots \\ \dots + \sigma d^2 \mathbf{C} \nabla_{\mathbf{xy}} \times \frac{\partial}{\partial t} \begin{bmatrix} \mathbf{B}_0(x, y, t) \\ \mathbf{B}_1(x, y, t) \\ \vdots \end{bmatrix} = \begin{bmatrix} \mathbf{0} \\ \mathbf{0} \\ \vdots \end{bmatrix} \end{aligned} \quad (3.21)$$

Here, the curl operator applies to the vectors indicated with a bold font, while the column vectors are used to separate the equations of the system.

In the spatial discretization, the vector-potential components are approximated by nodal shape functions $N_i, i = 1, \dots, N$, similarly to the static formulation. However, unlike in the static case with SV relativity, the stiffness matrix cannot be segregated because of the hysteretic material properties which allow the relativity to have any value between negative and positive infinity. Thus, the residual vector has to be formulated directly by applying the discrete curl operator

$$\mathbf{D}(x, y) = \begin{bmatrix} \frac{\partial N_1(x, y)}{\partial y} & \frac{\partial N_2(x, y)}{\partial y} & \dots & \frac{\partial N_N(x, y)}{\partial y} \\ -\frac{\partial N_1(x, y)}{\partial x} & -\frac{\partial N_2(x, y)}{\partial x} & \dots & -\frac{\partial N_N(x, y)}{\partial x} \end{bmatrix}. \quad (3.22)$$

The time discretization is performed with the Backward-Euler algorithm with a time-step length Δt . The discretized weak form for the m^{th} equation becomes

$$\mathbf{B}_m(x, y, t) = \mathbf{D}(x, y) \mathbf{a}_m(t) \quad (3.23)$$

$$\int_{\Omega_{\text{Fe}}} \mathbf{D}^T(x, y) \left[\frac{1}{d} \int_{-d/2}^{d/2} \mathbf{H}(\mathbf{B}(x, y, z, t)) \alpha_m(z) dz \dots \right. \\ \left. \dots + \frac{\sigma d^2}{\Delta t} \sum_{n=0}^{N_b-1} C_{mn} \mathbf{B}_n(x, y, t) \right] d\Omega = \mathbf{F}_m, \quad (3.24)$$

where \mathbf{F}_m includes values from the previous time step. The system is solved with the NR iteration. When the m^{th} subsystem is differentiated with respect to the n^{th} vector-potential component, the Jacobian matrix reads

$$\int_{\Omega_{\text{Fe}}} \mathbf{D}^T(x, y) \left[\frac{1}{d} \int_{-d/2}^{d/2} \frac{\partial \mathbf{H}}{\partial \mathbf{B}}(x, y, z, t) \alpha_m(z) \alpha_n(z) dz + \frac{\sigma d^2}{\Delta t} C_{mn} \right] \mathbf{D}(x, y) d\Omega.$$

To force the flux to stay inside the machine, the nodal values of the axial vector-potential components $A_n, n = 0, \dots, N_b - 1$ are set to zero at the outer boundary of the stator. In addition, the nodal values of the components $A_n, n = 1, \dots, N_b - 1$ are set to zero on the rotor side next to the solid-steel shaft in order also to ensure a unique solution on the rotor side.

In Publication IV, the effect of coupling the iron losses to the 2-D field solution was evaluated. For this purpose, the average flux-density distribution had to be solved when both coupling and not coupling the iron losses to its solution. In the *uncoupled model*, Equation (3.24) for the average vector potential A_0 was replaced by the traditional lossless FE formulation with SV materials (3.14):

$$\mathbf{S}(\mathbf{a}_0) \mathbf{a}_0 = \mathbf{0}, \quad \text{with } S_{ij}(\mathbf{a}_0) = \int_{\Omega_{\text{Fe}}} \nu(\mathbf{a}_0) (\nabla N_i) \cdot (\nabla N_j) d\Omega. \quad (3.25)$$

The rest of the equations were kept unchanged to obtain the iron losses in exactly the same manner as in the fully coupled model. In addition to full inclusion of the eddy currents and hysteresis into the solution, a study was made of the case where the eddy currents were included, but only the SV constitutive law was used. Thus these two coupled models are referred to as the *coupled hysteretic model* and *coupled SV model*, respectively.

3.2.3 Other Core-Loss Components

The damper bars were modeled in a similar way to the squirrel-cage rotor winding in (Arkkio 1987). The voltage across the n^{th} bar is obtained as

$$u_{\text{db},n} = L_{\text{db,ew}} \frac{di_{\text{db},n}}{dt} + R_{\text{db}} \left(i_{\text{db},n} + \sigma_{\text{db}} \int_{\Omega_{\text{db},n}} \frac{dA_0}{dt} d\Omega \right), \quad (3.26)$$

where $L_{\text{db,ew}}$ is the end-winding inductance, R_{db} is the bar resistance, $i_{\text{db},n}$ is the current in the bar and the integration is performed only over the

bar in question. For the short-circuit rings, a voltage equation is derived using analytically estimated inductance and resistance values, which are different for the parts of the rings connecting two adjacent poles and two adjacent bars on the same pole. The complete voltage equations for the damper winding are obtained by coupling the equations for each bar using Kirchoff's circuit laws.

The shaft was modeled as a solid conductor. The steel frame around the stator core was assumed to be of the same material as the shaft, but no circuit equations were applied between the shaft and the frame in order to allow eddy currents to be freely induced in these regions. The eddy-current loss densities in the damper windings, shaft, and the frame were calculated by integrating the square of the current density over the regions and multiplying by the conductivity of the region.

3.2.4 Numerical Details

All of the simulations described in Publications I, II, and IV-VI were performed using quadratic isoparametric triangular FEs. The numerical integrations in the 2-D domain were performed with Gauss integration using three integration points per element.

As described in Publication II, the 1-D integrations over the lamination thickness in (3.24) result in the cosine-series coefficients for the field strength \mathbf{H} . Thus these integrations were replaced by a fast cosine transform (FCT) algorithm performed to evaluate the coefficients of wave numbers $0, \dots, N_b - 1$. In the FCT, $2N_b + 1$ samples were taken in one half of the lamination in order to reduce the aliasing of the higher-order harmonics for these wave numbers. However, if $N_b = 1$, the flux density is constant and only one sample is enough. The integrations needed for the Jacobian matrix were obtained by performing the FCT for the differential reluctivity and calculating the integral of the resulting triple product of cosine terms analytically.

$N_\phi = 4$ directions were used in the vector hysteresis model throughout the work. A higher number could have been used for better accuracy, but the memory consumption of the FE model proved to grow too high and thus had to be reduced.

3.3 Calorimetric Measurement System

A calorimetric system was built for experimental determination of the electromagnetic losses of the 150-kVA synchronous generator used as a test machine. From the very beginning, it is emphasized that the purpose was not to implement a general test facility to be used in routine testing of different machines. Instead, the focus was kept on designing and calibrating the system for the individual test machine for which comprehensive loss measurements would be performed. The system has been discussed in more detail in Publication III, but the construction and operation of the system are briefly described below.

3.3.1 System Description

The test machine is a 150-kVA, 400-V, 4-pole synchronous generator originally designed for a diesel-generator application. The machine was modified by installing an additional drive-end (D-end) bearing for accurate coupling to an induction machine used for loading and driving purposes. In addition, the original brushless excitation machine was removed and slip rings were installed to allow accurate determination of the field current.

A schematic of the air-cooled open-cycle balance calorimeter built for the test machine is shown in Figure 3.2. The walls and ceiling were built of 50-mm Finnfoam[®] compressed polystyrene sheets attached to a planed board frame. The floor was a 70-mm Finnfoam sheet, on top of which a 30-mm plywood sheet was placed to equalize the force distribution. The construction was further strengthened by cutting holes in the polystyrene sheet under the fixing supports and filling those with pieces of glued laminated beam. The inside surfaces of the calorimeter were covered with 1-mm aluminum sheets to reflect radiating heat and to equalize the temperature distribution over the walls. The shaft hole was insulated by means of 9-mm cellular rubber sheets punched with exactly the same diameter as the shaft. In addition, the coupling between the test machine and the load/prime-mover machine was insulated by additionally surrounding it with 50-mm Finnfoam sheets.

The air inlet and outlet were placed on the ceiling, and the air flow was ensured by an exhaust fan placed after the outlet tube. The outlet air was blown outside to prevent excessive warming of the test hall. The fan of the test machine draws air from the non-drive end (N-end) to the D-end and

thus the outlet duct was placed above the D-end. The heater resistors used for the balance test were placed next to the N-end under the inlet duct.

3.3.2 Principles of Measurement

The total losses of the test machine are divided into friction and windage losses, stator- and field-winding resistive losses, and core losses, the last three of which comprise the electromagnetic losses to be measured:

$$P_{\text{loss}} = P_{\text{fw}} + P_{\text{Cu,s}} + P_{\text{Cu,r}} + P_{\text{core}} = P_{\text{fw}} + P_{\text{em}}. \quad (3.27)$$

During the test run, the power balance of the calorimetric system can be expressed as

$$P_{\text{loss}} = \Delta Q_t + q_t, \quad (3.28)$$

where ΔQ_t is the rate of change of the increase in thermal energy of the coolant flowing through the calorimeter, and q_t denotes the leakage heat not transferred by the coolant. During the balance test, the system is calibrated with heater resistors supplied with the power P_{res} , and the un-excited test machine is rotated with the prime mover. In this case, the power balance is

$$P_{\text{res}} + P_{\text{fw}} = \Delta Q_b + q_b. \quad (3.29)$$

Provided that the thermal power increase and the heat leakage are equal during the test run and the balance test ($\Delta Q_t = \Delta Q_b$ and $q_t = q_b$), the resistor power corresponds to the electromagnetic losses of the machine.

The thermal power is obtained as the product of the mass flow q_m and the increase in the coolant's enthalpy Δh when it is flowing through the calorimeter:

$$\Delta Q = q_m \Delta h. \quad (3.30)$$

The mass flow was obtained with an orifice-plate measurement in the outlet tube according to the standards EN ISO 5176-1 (2003) and EN ISO 5176-2 (2003). The enthalpy increase was obtained by measuring the inlet and outlet air temperatures and the inlet relative humidity, calculating the heat capacity, and multiplying by the temperature rise. More details on the measurements can be found in Publication III.

As also suggested by Zhang et al. (2011), the system was calibrated in advance to eliminate the need for a balance test after each test run. This was seen as justified since the total measurement time for the test run and the balance test could easily exceed 12 hours, and it is likely that the

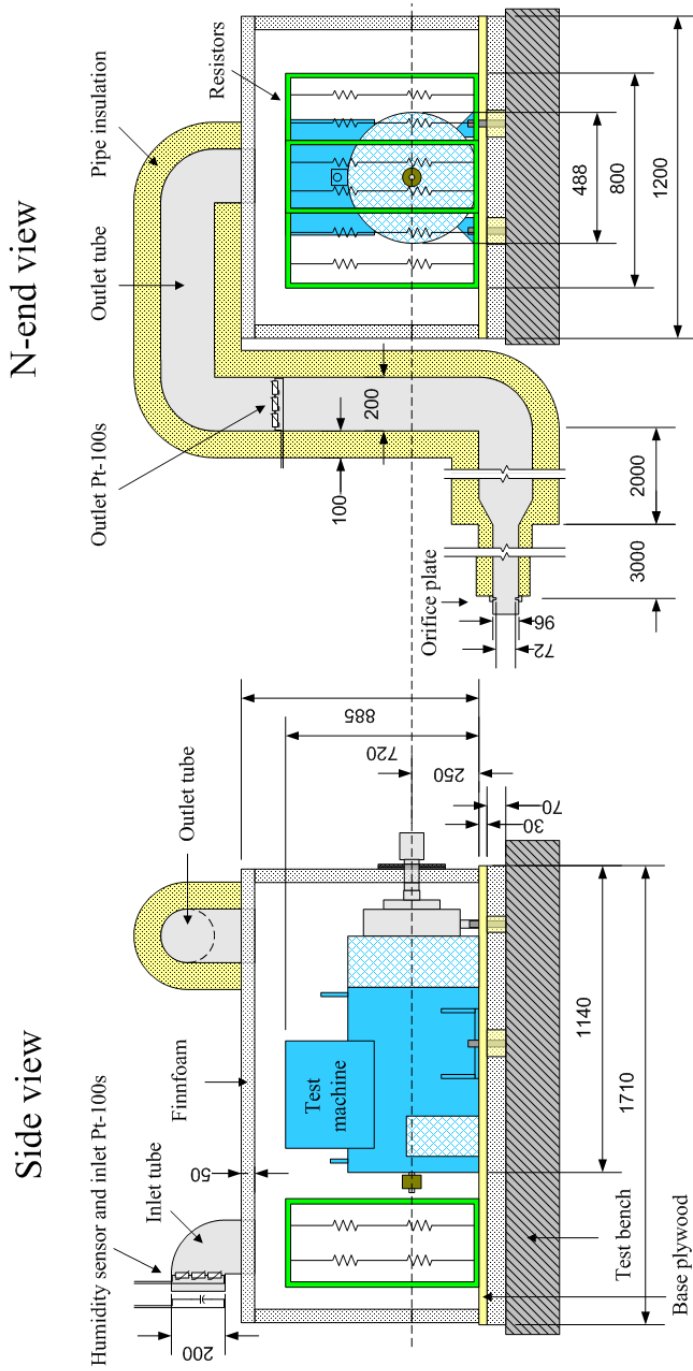


Figure 3.2. Schematic of the calorimetric system.

atmospheric pressure, the inlet air temperature, and the humidity contents of the coolant air would change during this period. Thus performing a separate balance test after each test run would not bring very much of an additional advantage when compared to the precalibrated system. The calibration measurements were performed by measuring the thermal power increase with resistor powers $1, 2, \dots, 13$ kW. On these points, the linear calibration curve shown in Figure 3.3 was fitted and used to evaluate the electromagnetic losses of the machine during the actual test runs.

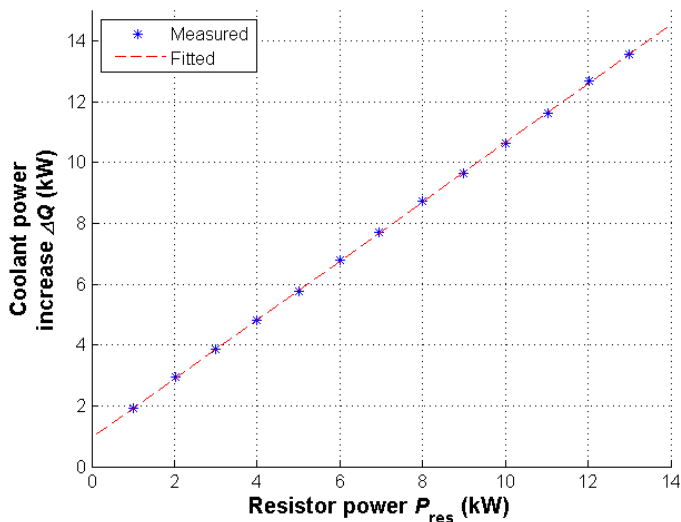


Figure 3.3. Measured points and fitted calibration curve.

The core losses were segregated from the total electromagnetic losses by subtracting the stator and field-winding resistive losses. The stator-winding losses were calculated using the measured effective stator currents and a resistance value obtained from a cooling-curve measurement. The cooling curves were determined by measuring the stator resistance during a period of two minutes after the machine had been switched off and stopped, and extrapolating to the switch-off instant assuming the winding to cool exponentially. The field-winding losses were determined directly from a DC power measurement.

3.3.3 Accuracy and Error Analysis

The balance test eliminates systematic errors in the air-property and the temperature measurements. However, since the thermal power increase during the test run has to be compared to that of the calibration curve,

the main sources of error in the system are

- Inaccuracy in the mass-flow measurement.
- Inaccuracy in the enthalpy measurement.
- Difference in the leakage conditions between the test run and the balance test.

The inaccuracies for the mass-flow and enthalpy measurements were determined by calculating the combined standard uncertainties (CSU) based on the errors of the sensors. MATLAB[®] was used to symbolically derive the equations for the mass flow and enthalpy, as well as the partial derivatives of these with respect to the measured quantities. Due to the dependency of the Reynolds number on the mass flow itself (Publication III), the mass-flow equations could not be derived in a closed form. However, the expression for the mass flow, for which the CSU was calculated, had been formed by symbolically performing one round of the iteration for the Reynold's number. By imposing small differences on the measured quantities, it was numerically ensured that the used expression yielded the CSU with an error of less than 1 %¹.

The leakage difference between the test run and the balance test is caused by the different physical location of the heat source inside the calorimeter. This difference was evaluated by performing additional calibration measurements taking advantage of the possibilities of supplying the calibration resistors from the test machine, as well as running the test machine in short-circuit operation with significant resistive losses. In the latter case, the heat distribution corresponds to that during the actual test run, while the former case is relatively close to the balance test. The total loss powers in these two cases were measured by using a calibrated torque transducer, and the heat leakages were calculated by (3.28). A more detailed description of this method is given in Publication III.

¹This means 1 % of the absolute error value, not one percentage point in the relative error.

4. Application and Results

In this chapter, the test machines used in the simulations and measurements are first described, and the results of the material identification are presented. After this, the numerical and experimental findings of publications I and IV-VI are summarized.

4.1 Studied Machines and Core Materials

Two different synchronous machines were used in the numerical simulations of Publications I and IV-VI. Machine I is a 12.5-MW 3150-V 6-pole synchronous motor for a variable-speed extruder application. Machine II is the 150-kVA 400-V 4-pole synchronous generator for which the calorimeter was designed and which was used to verify the simulations by comparison to measurements. The main data of the two machines are given in Table 4.1. The cross-sectional geometries and FE meshes of both machines can be found in Publication IV.

The stator slots of Machine II are axially skewed by one slot pitch, which cannot be taken into account in the 2-D FE model. According to the works of Karmaker and Knight (2005), Knight et al. (2009*a,b*) and Englebretson (2009), it is expected that the skewing increases the rotor losses as a result of the axial phase shift in the air-gap flux-density harmonics and the increased inter-bar currents flowing between the damper-winding bars. Zhan et al. (2009) modeled the inter-bar currents in a skewed machine by coupling a sliced 2-D model to a circuit representation of the bar-to-bar contacts. A similar approach could have been attempted here, but implementation of the slice model was considered to be beyond the scope of this work. In addition, as Englebretson concluded, determining a suitable value for the inter-bar resistance is very difficult since the bar-to-iron contacts are very statistical in their nature. They are also likely to be affected

by thermal expansion of the iron and the bars as well as centrifugal forces during actual operation.

For Machine II, three prototype rotors were manufactured from different materials. Rotor 1 was stacked of 0.5-mm Fe-Si electrical steel sheets, the same as those used as the stator material. Rotors 2 and 3 were stacked of 1-mm and 2-mm uninsulated steel plates, respectively. The measured electrical conductivities and the excess-loss coefficients obtained by scaling¹ the value in Publication II for the materials are summarized in Table 4.2. The measured static major hysteresis loops, some analytically modeled minor loops, and the SV curves are shown in Figure 4.1.

Table 4.1. Main data and dimensions of the studied machines.

Data	Machine I	Machine II
Machine type	motor	generator
Power	12500 kW	150 kVA
Voltage	3150 V	400 V
Current	2291 A	217 A
Displacement factor	1	0.8 cap
Frequency	50 Hz	50 Hz
Connection	star	star
Number of pole pairs	3	2
Stator outer diameter	1820 mm	430 mm
Stator inner diameter	1340 mm	300 mm
Air gap	15 mm	1.2 mm
Number of stator slots	90	48

Table 4.2. Core materials for Machine II and its prototype rotors.

Core part	Sheet thickness (mm)	Sheet conductivity (MS/m)	Excess-loss coefficient ($\text{W/m}^3(\text{s/T})^{3/2}$)
Stator / Rotor 1	0.5	3.00	0.718
Rotor 2	1.0	7.61	1.144
Rotor 3	2.0	7.85	1.162

¹The scaling was explained in the third paragraph of Section 3.1.3.

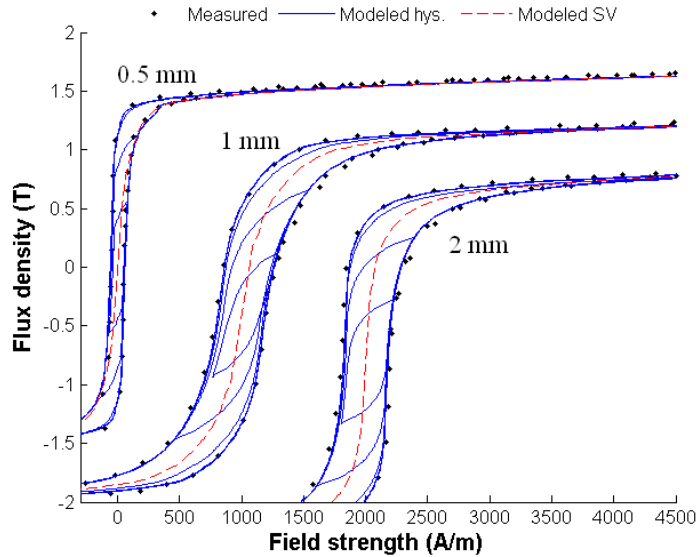


Figure 4.1. Measured major loops and modeled minor loops and SV curves for the three materials. The 1-mm and 2-mm curves are shifted from the origin for clarity.

4.2 Verification of the Model at No Load and Short Circuit

Publication VI presents verification of the electrical machine model in no-load and short-circuit operation. The open-circuit operation of a wound-field synchronous machine is a good operating point for verifying the material properties, since no stator resistive losses are present and the relationship between the field current and the terminal voltage is determined by the geometry and the material properties alone. The short-circuit operation is not very much affected by the material properties, but can be used to show that the windings and voltage equations are modeled correctly.

Figure 4.2 presents the no-load and short-circuit curves for Machine II with the three rotors. The measured curves and the ones obtained from time-stepping simulations with the SV material properties are shown. A good correspondence can be seen between the measured and simulated results. As expected, the short-circuit curves are almost unaffected by the rotor material. The biggest differences in the no-load curves can be seen in the knee points of the curves.

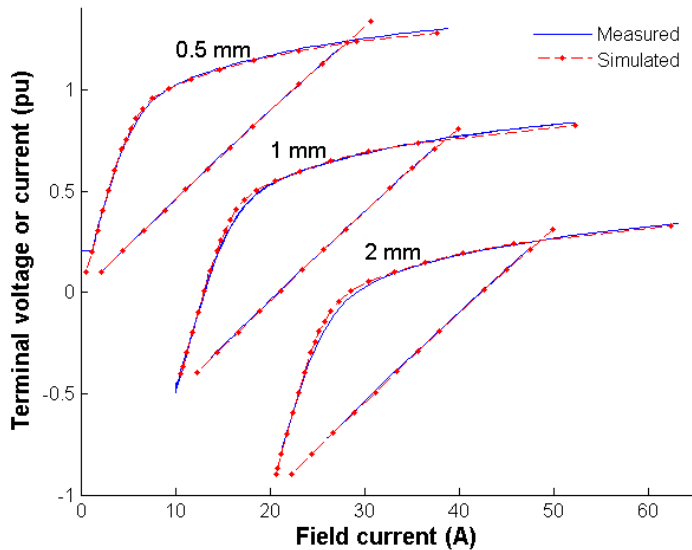


Figure 4.2. Measured and simulated no-load and short-circuit curves for Machine II. The 1-mm and 2-mm curves are shifted from the origin for clarity.

4.3 Effect of Iron Losses on the Field Solution

Publication IV presents an evaluation of the effects of the iron losses on the FE field solution. The need for the study arose from the problems encountered, especially, when including hysteretic material properties in the FE solution. When performing the simulations for Publication II, the convergence of the NR iteration was found to be very sensitive to the smoothness of the Everett function and the number of data points from which its values are interpolated during the computation. On the other hand, the hysteresis losses themselves could be sufficiently estimated from much rougher Everett data if the convergence problems could be avoided, for instance, by using SV materials during the computation. Another motivation was the fact that the size of the FE system and thus the computation time increases significantly when more skin-effect basis functions are considered in the iron-loss model. To compromise between the accuracy and computation time, the minimum sufficient number of basis functions had to be defined.

In the study, Machines I and II were simulated with DTC and PWM supplies, respectively. The simulations were performed using the *coupled hysteretic, coupled SV* and *uncoupled models*¹, and the differences in the

¹The three models were explained at the end of Section 3.2.2.

losses, electrical quantities and the electromagnetic torques predicted by these three models were compared. The effect of the coupling on the core losses of the two machines is summarized in Figure 4.3. The rotor losses can be seen to be reduced by 45-55 % when the accuracy of the skin-effect modeling is improved by increasing the number of basis functions N_b . The stator losses are almost constant irrespective of the number of basis functions. The slight decrease in the hysteresis losses with $N_b \geq 2$ is explained by the increasing number of sample points when the skin-effect terms are increased. To reduce memory consumption during the computation, the hysteresis losses are calculated in the same $2N_b + 1$ sample points as are used to form the FCT for the 1-D integration. The hysteresis losses are calculated by integrating the product of the field strength and the time derivative of the flux density over the lamination thickness. Thus, even if increasing the number of skin-effect terms above $N_b \geq 2$ does not significantly contribute to the accuracy of the skin-effect approximation, the accuracy of the hysteresis loss estimation improves because of the increasing number of sample points. Indeed, as the number of basis functions is increased, the hysteresis losses can be seen to approach the value obtained with $N_b = 1$, in which case only one sample point is needed to obtain the losses accurately. The results imply that using the classical low-frequency approximation, i.e., only one skin-effect basis function, is sufficient to predict the stator iron losses. On the rotor side, at least $N_b = 3$ basis functions should be used in order to predict the eddy-current losses accurately.

Figure 4.3 also shows that on the rotor side, the core losses obtained with the *coupled hysteretic* and *coupled SV models* are close to each other, while the *uncoupled model* yields somewhat larger losses. This means that in the rotor, the effect of the eddy currents on the FE solution is more significant than that of the hysteretic materials. On the stator side, the hysteresis losses have a greater effect due to smaller eddy-current losses, but the relative effect on the stator losses is smaller than that of the eddy currents on the rotor side. The effect on the total core losses of the machine is thus strongly influenced by the ratio of the stator and rotor core losses. If the rotor losses are dominant as in Machine II, the effect of the eddy-current losses on the field solution overrides that of the hysteretic materials. On the other hand, if the stator losses exceed the rotor losses, as in Machine I, the hysteretic materials have a more significant effect on the total core losses than the eddy currents, but the relative influence

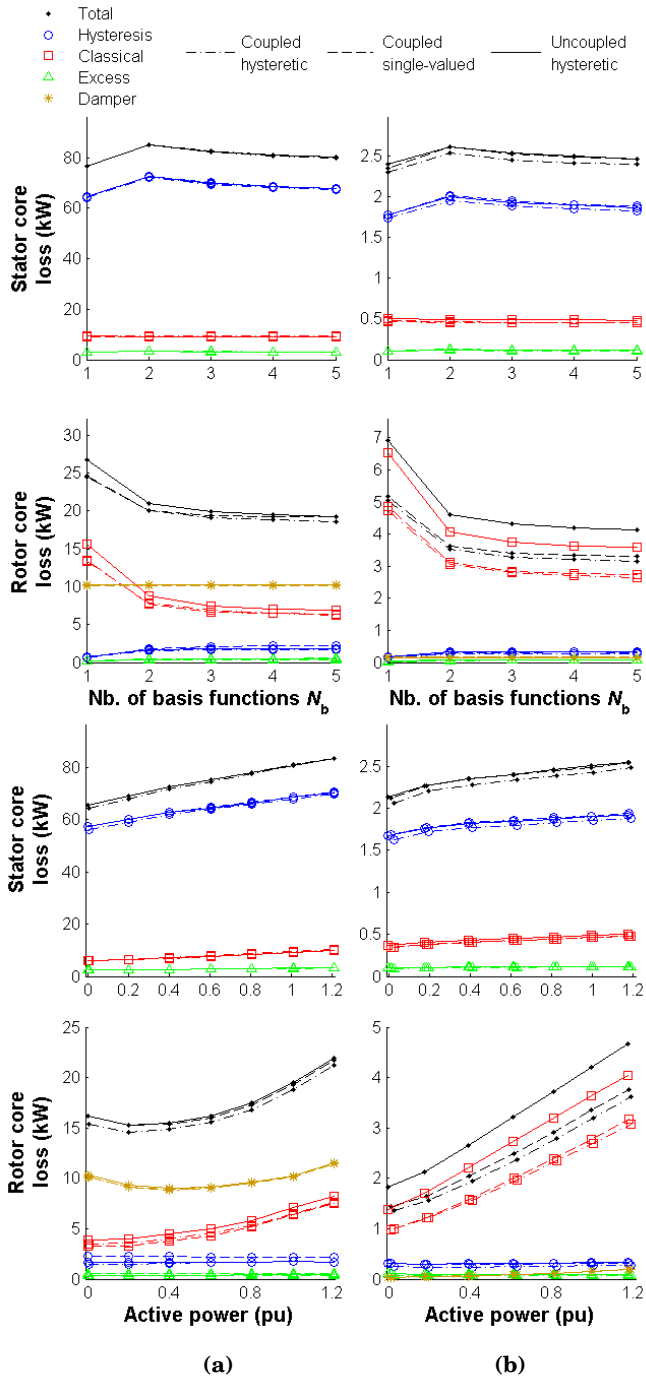


Figure 4.3. Dependence of the core losses on the number of skin-effect basis functions at the rated load, and on the load with $N_b = 4$ skin-effect terms.
 (a) Machine I and (b) Machine II.

remains small. Neglecting the hysteresis losses from the field solution is thus considered justified in order to improve the convergence properties of the FE model.

Table 4.3 compares the computation times of the *coupled hysteretic* and *coupled SV models* for the two machines. The computation times for the *SV model* with $N_b = 3$ skin-effect terms were 0.46 s and 0.6 s per time step for Machines I and II, respectively, and the model can be considered to be computationally efficient. For the *coupled hysteretic model*, the computation times are significantly higher. In the SV case, the dependency of the computation time on the number of skin-effect basis functions is quadratic, while in the hysteretic case the dependency is somewhat more linear.

The electrical operating points of the machines were found to stay almost equal despite the inclusion of the iron losses in the solution. Subsequently, when the iron losses were uncoupled from the solution, the electromagnetic torques and output powers were increased owing to the reduced power consumption in the machines. The total harmonic distortion contents in the terminal currents were also slightly reduced as a result of the increased transient inductances encountered by the flux of the machine.

Table 4.3. Computation times of the *coupled hysteretic* and the *coupled SV models* with the two machines and different numbers of skin-effect basis functions.

Average time per time step (s)		Nb. of skin-effect terms				
		1	2	3	4	5
Machine I	Hys.	0.27	1.15	1.98	2.94	4.05
	SV	0.13	0.28	0.46	0.71	1.09
Machine II	Hys.	0.21	0.95	1.61	2.28	3.22
	SV	0.11	0.31	0.60	1.01	1.60

4.4 Core-Loss Studies in Synchronous Machines

Core losses in wound-field synchronous machines were studied in Publications I and VI. In Publication I, a purely numerical study of the additional inverter-induced eddy-current losses in Machine I was performed, while Publication VI presented both experimental and numerical results on the core losses in Machine II. In both papers, the additional inverter losses

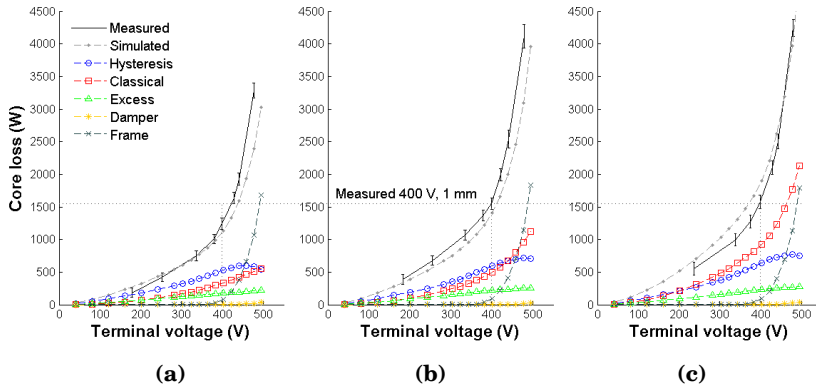


Figure 4.4. Measured and simulated core losses in Machine II at open-circuit operation. (a) 0.5-mm, (b) 1-mm and (c) 2-mm rotors.

were found to consist mostly of rotor eddy-current losses, which confirms the importance of modeling the rotor laminations.

Publication VI first presented the core losses for Machine II in open-circuit operation as a function of the terminal voltage. The results are summarized in Figure 4.4 for all three rotors. With the 0.5-mm sheet the simulated losses correspond relatively well to the measured ones. When the rotor sheet is changed to the 1-mm sheet, very similar relative increases are observed in the measured and simulated losses at 400 V. The frame losses can be seen to be extremely significant in both cases. The accuracy of the simulation results obviously suffers from the fact that the magnetization properties and conductivity of the frame were not measured. However, the 2-D model seems to be an appropriate tool to estimate the losses in the frame. A more detailed verification of the frame losses was presented in Publication VI.

When the rotor sheet is changed from the 1-mm sheet to the 2-mm one, the measured losses are almost unaffected. This is an interesting finding which was first thought to imply that the uninsulated lamination stacks tend to behave more like solid blocks than like ones with zero axial conductivity. However, the measurements of the axial conductivities of the 1-mm and 2-mm lamination stacks described in Publication VI revealed that the contact resistances between the laminations are also significant and very statistical in nature. Indeed, even the minimum average axial resistivities obtained from the measurements were around 1000 times larger than the resistivities of the lamination steels themselves. As discussed in the publication, another factor that may cause the losses to be equal is that the 2-mm sheets were cut by wire cutting while the 1-

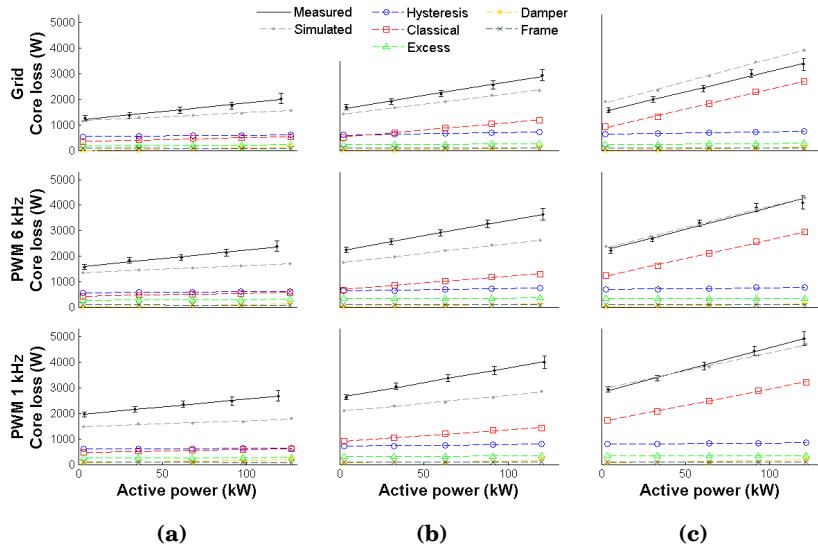


Figure 4.5. Measured and simulated core losses in Machine II with grid and inverter supply. (a) 0.5-mm, (b) 1-mm and (c) 2-mm rotors.

Table 4.4. Measured differences (a) in rated-load core losses compared to the 0.5-mm grid-supplied case and (b) between the rated-load and no-load core losses.

	(a)			(b)		
	0.5 mm	1 mm	2 mm	0.5 mm	1 mm	2 mm
Grid	0 %	45 %	66 %	63 %	76 %	125 %
6 kHz	19 %	80 %	103 %	56 %	65 %	94 %
1 kHz	33 %	97 %	142 %	39 %	55 %	71 %

mm sheets were punched. Punching is known to increase the iron losses through deterioration of the magnetization properties of the sheets. Thus it seems possible that the losses occurring close to the surface of the rotor have significantly increased in the 1-mm sheets and are thus close to those of the 2-mm sheets.

The results obtained in loaded operation are summarized in Figure 4.5 and Table 4.4. Table 4.4a shows numerical values of the differences between the measured rated-load core losses, compared to the 0.5-mm grid-supplied case. It can be seen that using thicker steel sheets significantly increases the total core losses even with grid supply, and that the effect is even more severe with inverter supply and with lower switching frequencies. The differences between the measured rated-load and no-load core losses for all three rotors and both for grid and inverter supply are shown in Table 4.4b. The effect of the loading on the core losses can be

seen to decrease when the voltage waveform deteriorates. Figure 4.5 also shows that the slopes of the lines fitted to the measured losses are almost unaffected by the supply, while the constant losses increase as a result of changing to inverter supply and reducing the switching frequency.

Segregation of the losses reveals that the increases in the iron losses as a result of both loading and the inverter supply are mostly caused by eddy currents induced on the rotor side. Similarly to the recent observation of Shisha et al. (2012) for solid-rotor synchronous machines, the loading of the machine causes the iron losses to concentrate on the leading edge of the pole shoe. For Machine II, this is illustrated in Figure 4.6a. The additional inverter losses, however, occur mostly on the lagging edge of the pole shoe, as shown in Figure 4.6b. In Publication I, this was explained for Machine I by the fact that as a result of the saturation of the leading edge of the pole, its permeability is decreased which reduces the skin effect of the higher-order harmonics when compared to the lagging edge. However, as also discussed by Shisha et al., a more likely explanation is that the unsaturated lagging edge simply offers an easier path for the high-frequency harmonics having a wave length equal to two pole pitches. When the high-frequency flux distributions of Machines I and II are compared in Figure 4.7a and Figure 4.7b, respectively, the effect can be seen to be much clearer for Machine II than for Machine I. However, the distribution also depends on the instantaneous values of the phase currents.

4.5 Study of Design Improvements

The possibilities of minimizing the additional inverter losses by changing the rotor pole geometry were studied in Publication V. The idea for this study arose after questioning the use of 2-mm steel plates in the rotors of inverter-supplied machines. This practice dates back to the time before power converters, when synchronous machines were used solely with grid supply and operated as generators or DOL motors. It thus seemed possible that other design practices for VSD applications may also have been transferred directly from the criteria set for the grid-supplied machines, and that different rules might be more suitable if the machines are supplied with non-sinusoidal voltages. The same was concluded earlier by Cao, Bradley, Clare and Wheeler (2010) for induction machines.

The study was made for Machine I, which was simulated with a mea-

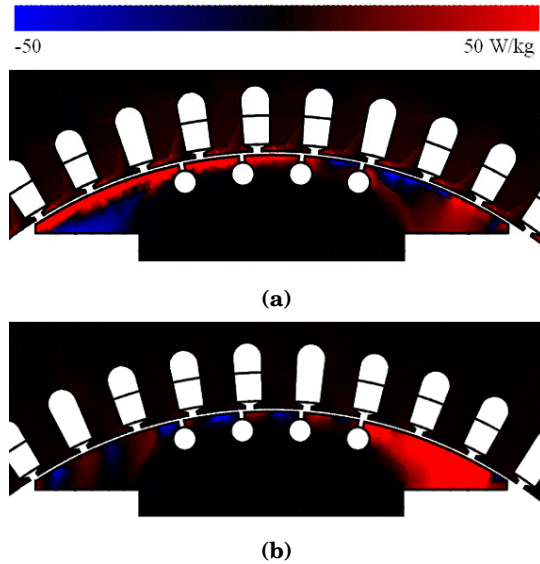


Figure 4.6. Differences in the iron-loss distributions in Machine II with the 1-mm rotor (a) between the rated-load and no-load operation points in the 1-kHz PWM case and (b) between the 1-kHz PWM supply and grid supply in the rated-load operation. Direction of rotation is counterclockwise.

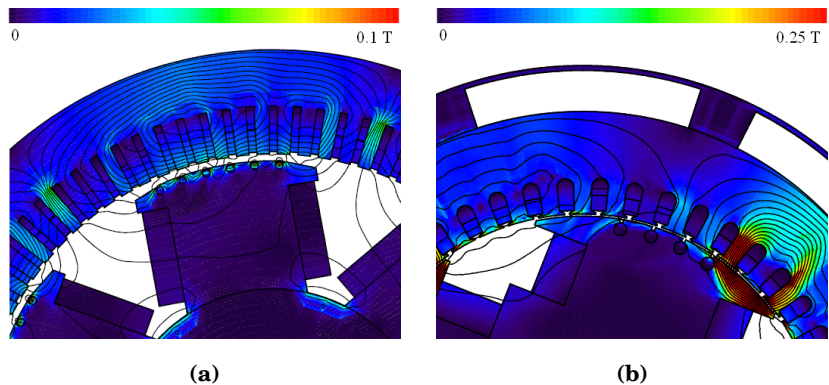


Figure 4.7. Instantaneous high-frequency fluxes in (a) Machine I and (b) Machine II. Direction of rotation is counterclockwise.

sured DTC voltage waveform and with the rotor stacked of the 2-mm sheets. The rotor pole shoe was assumed to have the shape of a circular segment with a certain width and radius. The air-gap length was defined as the distance between the stator and the center point of the pole shoe, and the shoe width and radius were limited by the field-winding width and the center-point radius. The total electromagnetic losses were calculated with several different combinations of the shoe width and radius with air-gap values ranging from 10 to 30 mm in 5-mm steps. The lowest rated-load losses were observed at an air-gap length of 20 mm, for

which Figure 4.8 shows the dependency of the losses on the shoe width and radius. Since the stator resistive losses were almost unaffected by the pole-shoe shape, only the sum of the field-winding copper losses and the core losses are shown. There is clearly an optimum value for both the width and the radius, at which the losses are at a minimum. Figure 4.9a shows the optimum pole geometry and the FE mesh used in the calculation. With this construction, the total electromagnetic losses were reduced by 5.2 % when compared to the original pole shoe. In general, increasing the air gap from its optimum value would increase the excitation losses but reduce the pole-surface iron losses. Reducing the air gap would have the opposite effect.

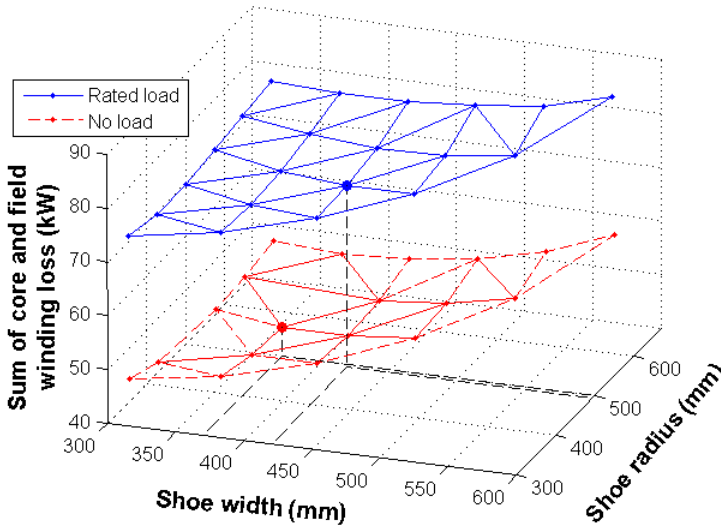


Figure 4.8. Sum of the field-winding and core losses with different shoe widths and radiuses at 20-mm air gap.

Next, the damper winding was modified. The effects of modifying the damper winding on the dynamic performance of the machine were not considered in this study. However, according to the works of Brass and Mecrow (1993) and Cao and Li (1994), it was concluded that a frequency-converter-supplied machine can maintain a reasonable transient performance and sufficiently low torque ripple, and thus the study was seen as justified, especially, when considering dynamically less demanding applications.

The distance of the damper winding from the pole-shoe surface was varied between 1 and 9 mm and the width of the slot opening between 2 and 15 mm, the diameter of the bar being 16 mm. The minimum losses were

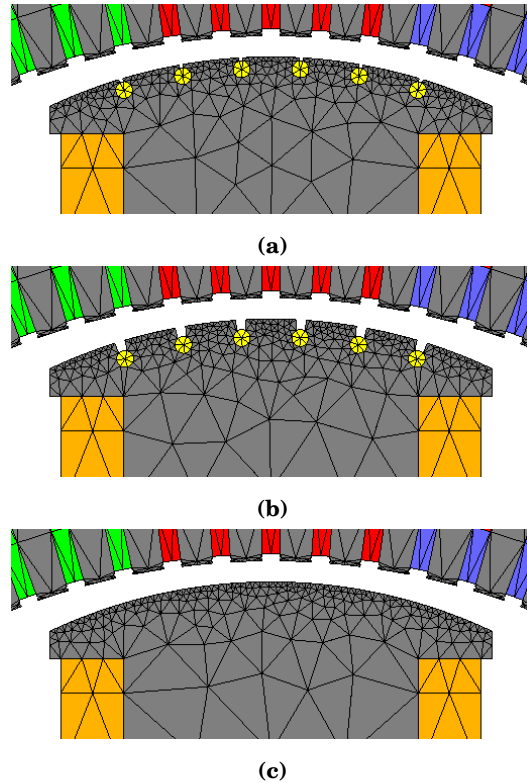


Figure 4.9. Modified rotor constructions: (a) modified pole shoe, (b) modified damper winding and (c) removed damper winding.

observed at the maximum studied depth of 9 mm and at a slot-opening width of 8 mm, which agrees with the findings of Stranges and Dymond (2003). This construction is shown in Figure 4.9b, and the electromagnetic losses were reduced by 6.8 % when compared to the original pole. Removing the damper completely (Figure 4.9c) resulted in a further decrease of 4.7 %, the difference from the original pole now being 11.2 %. Shifting the damper from the center line of the pole did not have a notable effect on the losses.

Finally, the effect of using Fe-Si sheets on the rotor was studied in the damperless case. As can be concluded from the experimental findings of Publication VI and the previous section, the core losses were significantly reduced as a result of changing to the lower-loss sheet. From the damperless case with the 2-mm rotor, the total electromagnetic losses were reduced by a further 4.7 %, and the reduction from the original pole-shoe construction rose to 15.4 %.

5. Discussion and Conclusions

This thesis has dealt with core losses of frequency-converter-supplied synchronous machines. In this chapter, the methods and obtained findings are summarized and discussed. Some practical engineering considerations and suggestions for further work are also presented.

5.1 Discussion of the Methods and Results

5.1.1 Summary of the Findings

Iron-Loss Model

The developed iron-loss model proved to be a suitable tool to estimate the iron losses in electrical machines by the 2-D FE method. The simulated no-load core losses for the induction machine in Publication II and the Fe-Si-rotor synchronous machine in Publication VI are close to the measured ones, which implies that the model works properly. The main difficulty in verifying the iron-loss model is that further segregation of the core losses into different components is impossible, or at least extremely challenging. However, all the loss components usually included in the stray-load losses are likely to be at a minimum in no-load operation, which reduces some of the differences between the numerical model and the actual machine. The observation made in Publication VI that the differences between the measured and simulated core losses increase with loading also supports this conclusion. Still, some inevitable differences are also caused in no-load operation by the deteriorated material properties and galvanic contacts between the core laminations resulting from punching, magnetic and electric anisotropy, and circulating currents in the stator parallel wires, which are not taken into account in the numerical model.

The global coupling using the nodal values of the vector potential ensures good computational performance since all the unknowns are solved from a single system of equations. In order to minimize the size of the equation system, it was concluded that a three-term cosine-series expansion is sufficient to predict the eddy-current losses on the rotor side. On the stator side, the classical low-frequency approximation neglecting the skin effect was found to be enough.

According to the results of Publication IV and Section 4.3, the effect of the hysteresis losses on the FE field solution is considered to be small enough to justify their omission from the solution. This allows SV material properties to be used during the solution which improves the convergence and reduces the memory consumption during the computation, since the hysteresis loops do not need to be stored at each 2-D and 1-D integration point. The hysteresis losses can be determined in the post-processing stage by using a suitable hysteresis model. Since the differential reluctivity is not needed, extra caution does not have to be taken to ensure the smoothness of the hysteresis loops and rougher data can be used to estimate the losses.

Calorimetric System

The calorimetric system was found to be an accurate method for determining the core losses of the test machine. A good enough measurement accuracy was obtained in order to distinguish the effects of the rotor sheet material on the core losses of the test machine. It is likely that the measurement error resulting from the input-output method would have been too large for this purpose. The error of the calorimetric system is mostly caused by the errors in the temperature and differential pressure measurements, and thus the accuracy could still easily be improved by replacing the sensors by more accurate ones.

Another method for determining the measurement error of the calorimetric system would be to calculate the standard deviation of numerous measurements for the same operating point. However, since the inlet temperature is not controlled, the losses of the test machine are likely to vary if the temperature changes between the tests. A similar study could be performed with the calibrating resistors by keeping the power constant with a suitable control system.

For routine testing of machines, a calorimetric system may seem to be too complex and slow an arrangement. As pointed out in Publication III,

however, the input-output measurement should also be performed only after the steady thermal state has been achieved. Thus the difference in the measurement times between the calorimetric method and the input-output method is actually much smaller than generally expected. In addition, accurate measurement of torque requires choosing a torque transducer with a full-scale range close to the expected torque to be measured. Thus, especially if the machine is to be tested in different loading points, several different torque transducers are needed for the measurements. This increases the costs of the testing facility, and the testing time for a single machine increases if the torque transducers have to be changed.

Core Losses in Synchronous Machines

The measurement results showed that the use of 0.5-mm Fe-Si laminations should be seriously considered for inverter-supplied machines to reduce their losses. With the increasing drive for energy efficiency and constantly tightening efficiency limits, many different measures may have to be undertaken to minimize the losses. Based on the results of this thesis, it is carefully suggested that many old design practices previously applied to generators and DOL motors could be looked through and possibly reconsidered for inverter-fed applications. The simulations of Publication V showed that modification of the rotor pole-shoe geometry alone led to a 5.2 % decrease in the total electromagnetic losses. For dynamically less demanding applications, the possibility of removing the damper winding should also be clarified.

If the iron-loss model is assumed to work correctly, the differences between the measured and modeled core losses at higher loads have to be explained by other means. The problem of the inter-bar currents is challenging as a result of the very random nature of the bar-to-iron contact resistances. However, with suitable models, statistical analysis could be applied to predict the possible range of variation in the losses caused by the inter-bar currents. In addition, the effect of frequency-converter supply on these losses has not been studied earlier.

3-D models would be needed to study the eddy-current losses in the end regions of the machines. Although Karmaker (1992) assumed the end-region losses to be included in the no-load core losses, these may also be affected by the loading especially in random-wound machines, in which the winding ends are relatively close to the core. To estimate the losses in the frame, the 2-D FE model can be concluded to be sufficient.

5.1.2 Significance of the Work

The developed iron-loss model comprised a mesh-free lamination eddy-current loss model coupled to models for vector hysteresis and the local excess eddy currents. According to the literature review of Chapter 2, the homogenization approaches used earlier have considered only single-valued materials, and coupling to hysteretic material properties has not been presented before. In addition, the earlier models based on the FE solution of the 1-D diffusion problem have been coupled to the 2-D FE solution in a local manner at each integration point of the 2-D geometry. In this work, global coupling was applied by expressing the axial dependency of the flux density as a series expansion of magnetic vector-potential components which were approximated by nodal shape functions. When 2nd- or higher-order finite elements are used, the number of nodes is typically lower than the number of integration points, which makes the developed model more efficient when compared to a locally coupled one.

A comprehensive study was performed on the effects of including the iron losses in the FE field solution of synchronous machines. Earlier, one similar study has been performed for induction machines but otherwise the topic has received very little attention in the literature. It was shown that the computational performance of the developed model can be significantly improved by omitting the hysteresis losses from the field solution and minimizing the number of skin-effect terms to a level which still yields sufficient accuracy. This is an important finding which leads to a significant reduction in computation time when estimating the core losses of synchronous machines by numerical simulations.

The calorimetric system built during this work is larger than most of the implementations presented earlier in the literature. The calorimeter was applied for comprehensive testing of a 150-kVA synchronous machine with rotors stacked of three different materials and both grid and frequency-converter supply. Earlier reports on loss measurements with different rotor materials could not be found during the literature review.

In the earlier works reviewed in Chapter 2, the effect of the inverter on the core losses of laminated-core synchronous machines was not studied very much but considered rather insignificant and uninteresting. However, in this work it was shown that laminated-core machines are also significantly affected by the frequency-converter supply, and that the sheet material has a major influence on the total core losses of the machine.

Knowledge of the iron-loss distributions in the machines and the structural design modifications studied during this work can be applied to design more energy-efficient synchronous machines. The design improvements of a high-power synchronous motor allow large absolute energy savings not only in the machine itself but also in the whole energy conversion and transmission chain, which transfers the energy of a primary source into the mechanical work done by the machine. On the other hand, more accurate measurement techniques make it possible to verify the efficiency improvements, which is necessary to tighten the efficiency limits by standardization. From these perspectives, the results of the work can be seen as a contribution to the constant strive for cleaner technology.

5.1.3 Engineering Considerations

Applicability of the Iron-Loss Model

Owing to its relatively good computational efficiency, the developed iron-loss model can be considered suitable for everyday design purposes. The fully coupled loss model with several skin-effect basis functions may still be too heavy for practical use, but advantage may be taken of the results of Publication IV. First of all, the hysteresis and excess losses can be calculated in the postprocessing stage without a significant loss of accuracy. Second, the best performance is obviously obtained when only one skin-effect basis function is used. This case corresponds to the classical low-frequency approximation omitting the skin effect, and tends to overestimate the iron losses due to the reduced damping effect. However, extra core losses are caused in real machines by the eddy currents in the support structures and the circulating currents in the parallel branches of the windings. These losses are usually not accounted for in 2-D FE models, and thus the overestimation of the iron losses tends to correct the total estimated losses in the right direction. For practical design purposes it is often more convenient for the model to slightly overestimate the losses rather than to give too optimistic results.

The traditional lossless vector-potential formulations can easily be updated to take into account the classical low-frequency eddy-current losses by replacing the single-valued reluctivity ν by the operator

$$\nu + \frac{\sigma d^2}{12} \frac{\partial}{\partial t},$$

and also discretizing the time derivative in the laminated regions. Implementation of the full model is more complicated, especially in low-level FE

implementations, in which the system matrix is formed in a rather fixed manner and modification of the equation system is difficult.

Calorimetry for Routine Testing

The calorimetric method can achieve a very good measurement accuracy for the total electromagnetic losses. For motor and generator manufacturers accurate loss measurements are important since when the losses are known accurately, the reduction of safety margins leads to cost savings in construction materials and cooling arrangements. A few requirements for a calorimeter designed for routine machine testing in factories can be suggested, as follows:

- The construction should allow easy and fast assembly and disassembly of the system. Fixed wiring installations and an adjustable or changeable arrangement for the through-hole of the shaft are needed to reduce leakage differences between tests and to allow the testing of different sizes of machines.
- Premeasured calibration curves should be used to shorten the time required for testing.
- A large calorimeter volume with respect to the size of the test machine would be advantageous in order to reduce the differences in the leakage conditions between the calibration measurements and different test machines.
- Due to long thermal time constants of large machines, the coolant inlet temperature should be controlled in order to prevent variations in the thermal conditions during the course of both the calibration measurements and the test runs.
- If possible, an automatically controlled preheating system could be used to force the calorimeter temperature to the steady state as quickly as possible. This can be achieved by applying a higher loss power at the beginning of the test and reducing the extra loss when the temperature increases. If implemented correctly, this could significantly reduce the measurement time.

5.2 Suggestions for Future Work

5.2.1 Global versus Local Coupling of Eddy Currents

In this work, the eddy currents were coupled to the 2-D field solution by using global coupling. This was implemented by expressing the axial dependency of the flux density in the lamination as the curl of a truncated Fourier series of axial magnetic vector-potential components. Using vector potentials ensures that the flux-density components and thus also the total flux-density distribution are divergence-free. In earlier works presented in the literature, the coupling has been implemented locally by calculating the axial flux-density distribution separately at each integration point of the 2-D geometry. Although not mentioned earlier in this thesis, a brief study was performed during this work to study the possible differences between the implemented global model and a local approach, in which system (3.6) for the 1-D diffusion problem was solved locally at each 2-D integration point separately. Slightly surprisingly, the global and local solutions for the higher-order flux-density components proved to be unequal. Using 1st-order FEs ensuring a constant flux density in each 2-D element, it was found that the flux-density components obtained from the local model were not divergence-free on the boundary of two adjacent elements. On the contrary, the divergence of the flux-density components solved from the global model was also zero also at the boundary as a result of using the vector-potential formulation. At least in the studied geometry, however, the eddy-current losses were found not to vary significantly between the two formulations. Either way, this is an interesting finding from the numerical point of view, and could provide a topic for a more systematic study.

5.2.2 Eddy Currents in Uninsulated Lamination Stacks

The open-circuit measurements of Publication VI did not show any increase in the total core losses when the rotor lamination was changed from the 1-mm steel plate to the 2-mm one. The initial conclusion from this was that the steel-plate rotors behave more like solid rotors than ones with zero axial conductivity. However, the measurements of the average axial conductivities of the steel-plate lamination stacks showed that the contact resistances between the laminations are significant and also

very statistical in nature. Oxide layers, dust, dirt, and grease insulate the laminations from each other in a very random manner and thus accurate modeling of the stacks is challenging. In addition, the insulating layers are likely to be very thin when compared to the thickness of the laminations, which would require an extremely dense FE meshing or alternatively using a thin shell model for imperfect insulating layers. The development of such a model would allow numerical statistical studies of the distribution of eddy currents in the stacks of uninsulated laminations, and would give at least some insight into the actual behavior of the rotor losses.

5.2.3 Effects of Manufacturing on the Core Losses

Physical iron-loss models make it possible to perform more accurate studies on the effect of manufacturing processes on the core losses. As acknowledged in Publication VI, one major factor affecting the iron losses is that the magnetic material properties deteriorate as a result of residual stresses and plastic strains imposed in the cores by punching of the laminations as well as shrink-fitting, pressing and welding of the core. If the skin effect is modeled accurately, the magnetization properties obviously also have an effect on the classical eddy-current losses. However, e.g., in (Permiakov et al. 2004), using the statistical theory of Bertotti (1988) led to the conclusion that the eddy-current losses remain unchangeable under elastic stresses and vary only slightly with plastic strains, while the credit for increasing the losses was given to the excess losses. Following the example of Mayergoyz and Serpico (1999), it is reasonable to state that in reality at least part of the increase in the iron losses could be caused by a change in the classical eddy-current losses resulting from deterioration of the magnetization properties. The brief numerical study made by Rasilo et al. (2012) gives some support for this statement. However, a more comprehensive study on the topic could also be performed.

5.3 Conclusions

As a summary, a competitive physical iron-loss model was developed during this work to be used within the 2-D FE analysis of laminated-core electrical machines. Together with calorimetric loss measurements, the model was applied to obtain important knowledge about core losses in

wound-field synchronous machines, their spatial distribution, and their dependency on the rotor sheet material and frequency-converter supply. As expected, the main difficulty encountered during the work was that the iron losses alone do not fully explain the total core losses obtained from the measurements. However, in the case of the 0.5-mm Fe-Si-rotor, the simulated losses are close to the measured ones which implies that the model works properly.

References

- Aarniovuori, L., Laurila, L. I. E., Niemelä, M. and Pyrhönen, J. (2012), 'Measurements and simulations of DTC voltage source converter and induction motor losses', *IEEE Trans. Ind. Electr.* **59**(5), 2277–2287.
- Adly, A. A. and Mayergoyz, I. D. (1993), 'A new vector Preisach-type model of hysteresis', *J. Appl. Phys.* **73**(10), 5824–5826.
- Albach, M., Durbaum, T. and Brockmeyer, A. (1996), Calculating core losses in transformers for arbitrary magnetizing currents a comparison of different approaches, in 'Annual IEEE Power Electronics Specialists Conference (PESC)', Vol. 2, Baveno, Italy, June 1996, pp. 1463–1468.
- Arkio, A. (1987), Analysis of Induction Motors Based on the Numerical Solution of the Magnetic Field and Circuit Equations, PhD thesis, Helsinki University of Technology, Espoo, Finland.
- Aston, K. and Rao, M. K. (1953), 'Pole-face losses due to open slots on grooved and ungrooved faces', *Proc. IEE IV* **100**(5), 104–113.
- Atallah, K. and Howe, D. (1993), 'Calculation of the rotational power loss in electrical steel laminations from measured B and H', *IEEE Trans. Magn.* **29**(6), 3547–3549.
- Bergqvist, A. (1996), 'A simple vector generalization of the Jiles-Atherton model of hysteresis', *IEEE Trans. Magn.* **32**(5), 4213–4215.
- Bertotti, G. (1985), 'Physical interpretation of eddy current losses in ferromagnetic materials. I. Theoretical considerations', *J. of Appl. Phys.* **57**(6), 2110–2117.
- Bertotti, G. (1988), 'General properties of power losses in soft ferromagnetic materials', *IEEE Trans. Magn.* **24**(1), 621–630.
- Bottauscio, O. and Chiampi, M. (2002), 'Analysis of laminated cores through a directly coupled 2-D/1-D electromagnetic field formulation', *IEEE Trans. Magn.* **38**(5), 2358–2360.
- Bottauscio, O., Chiampi, M. and Chiarabaglio, D. (2000a), 'Advanced model of laminated magnetic cores for two-dimensional field analysis', *IEEE Trans. Magn.* **36**(3), 561–573.
- Bottauscio, O., Chiampi, M. and Chiarabaglio, D. (2000b), 'Magnetic flux distribution and losses in narrow ferromagnetic strips', *J. Magn. Magn. Mater.* **215-216**, 46–48.

- Bottauscio, O., Chiarabaglio, D., Chiampi, M. and Repetto, M. (1995), 'A hysteretic periodic magnetic field solution using Preisach model and fixed point technique', *IEEE Trans. Magn.* **31**(6), 3548–3550.
- Bradley, K. J., Cao, W. and Arellano-Padilla, J. (2006), 'Evaluation of stray load loss in induction motors with a comparison of input-output and calorimetric methods', *IEEE Trans. Energy Convers.* **21**(3), 682–689.
- Brainard, F. K. (1913), 'Notes on stray losses in synchronous machines', *Am. Inst. Electr. Eng. Trans.* **XXXII**(1), 519–521.
- Brass, M. and Mecrow, B. (1993), The role of damper circuits in field orientated synchronous drives, in 'Sixth International Conference on Electrical Machines and Drives, Oxford, UK, September 1993', pp. 115–120.
- Brockmeyer, A. and Schulting, L. (1993), Modelling of dynamic losses in magnetic material, in 'Fifth European Conference on Power Electronics and Applications', Brighton, UK, September 1993, pp. 112–117.
- Cao, L. Y. and Li, F. H. (1994), 'Damper windings in synchronous machines fed by a current-source inverter', *IEE Proc. Electr. Power Appl.* **141**(5), 229–234.
- Cao, S., Wang, B., Yan, R., Huang, W. and Yang, Q. (2004), 'Optimization of hysteresis parameters for the Jiles-Atherton model using a genetic algorithm', *IEEE Trans. Appl. Supercond.* **14**(2), 1157–1160.
- Cao, W. (2009), 'Comparison of IEEE 112 and new IEC Standard 60034-2-1', *IEEE Trans. Energy Convers.* **24**(3), 802–808.
- Cao, W., Asher, G. M., Huang, X., Zhang, H., French, I., Zhang, J. and Short, M. (2010), 'Calorimeters and techniques used for power loss measurements in electrical machines', *IEEE Instrum. Meas. Mag.* **13**(6), 26–33.
- Cao, W., Bradley, K. J., Clare, J. C. and Wheeler, P. W. (2010), 'Comparison of stray load and inverter-induced harmonic losses in induction motors using calorimetric and harmonic injection methods', *IEEE Trans. Ind. Appl.* **46**(1), 249–255.
- Cao, W., Bradley, K. J. and Ferrah, A. (2009), 'Development of a high-precision calorimeter for measuring power loss in electrical machines', *IEEE Trans. Instrum. Meas.* **58**(3), 570–577.
- Cao, W., Huang, X. and French, I. (2009), 'Design of a 300-kW calorimeter for electrical motor loss measurement', *IEEE Trans. Instrum. Meas.* **58**(7), 2365–2367.
- Carter, G. (1955), 'A note on the surface loss in a laminated pole-face', *Proc. IEE C* **102**(2), 217–220.
- Chari, M. and Silvester, P. (1971), 'Analysis of turboalternator magnetic fields by finite elements', *IEEE Trans. PAS* **90**(2), 454–464.
- Chen, J., Ma, W., Wang, D., Li, F. and Guo, Y. (2010), A new method for calculating iron loss based on Hilbert transform, in 'XIX International Conference on Electrical Machines (ICEM)', Rome, Italy, September 2010, pp. 1–5.

- Chiampi, M., Chiarabaglio, D. and Repetto, M. (1995), 'A Jiles-Atherton and fixed-point combined technique for time periodic magnetic field problems with hysteresis', *IEEE Trans. Magn.* **31**(6), 4306–4311.
- Chiampi, M., Negro, A. and Tartaglia, M. (1980), 'A finite element method to compute three-dimensional magnetic field distribution in transformer cores', *IEEE Trans. Magn.* **16**(6), 1413–1419.
- Del Vecchio, R. (1982), 'The calculation of eddy current losses associated with rotating magnetic fields in thin laminations', *IEEE Trans. Magn.* **18**(6), 1707–1709.
- Dlala, E. (2008a), Magnetodynamic Vector Hysteresis Models for Steel Laminations of Rotating Electrical Machines, PhD thesis, Helsinki University of Technology, Espoo, Finland.
- Dlala, E. (2008b), 'A simplified iron loss model for laminated magnetic cores', *IEEE Trans. Magn.* **44**(11), 3169–3172.
- Dlala, E. (2011), 'Efficient algorithms for the inclusion of the Preisach hysteresis model in nonlinear finite-element methods', *IEEE Trans. Magn.* **47**(2), 395–408.
- Dlala, E. and Arkkio, A. (2007), 'Measurement and analysis of hysteresis torque in a high-speed induction machine', *IET Electr. Power Appl.* **1**(5), 737–742.
- Dlala, E. and Arkkio, A. (2009), 'A general model for investigating the effects of the frequency converter on the magnetic iron losses of a squirrel-cage induction motor', *IEEE Trans. Magn.* **45**(9), 3303–3315.
- Dlala, E., Belachen, A. and Arkkio, A. (2008), 'Inverted and forward Preisach models for numerical analysis of electromagnetic field problems', *Physica B Condens. Matter* **403**(2-3), 428–432.
- Dlala, E., Belachen, A. and Arkkio, A. (2008a), 'Efficient magnetodynamic lamination model for two-dimensional field simulation of rotating electrical machines', *J. Magn. Magn. Mater.* **320**(20), 1006–1010.
- Dlala, E., Belachen, A. and Arkkio, A. (2008b), 'A fast fixed-point method for solving magnetic field problems in media of hysteresis', *IEEE Trans. Magn.* **44**(6), 1214–1217.
- Dlala, E., Belachen, A. and Arkkio, A. (2010), 'On the importance of incorporating iron losses in the magnetic field solution of electrical machines', *IEEE Trans. Magn.* **46**(8), 3101–3104.
- Dlala, E., Belachen, A., Fonteyn, K. and Belkasim, M. (2010), 'Improving loss properties of the Mayergoyz vector hysteresis model', *IEEE Trans. Magn.* **46**(3), 918–924.
- Dlala, E., Belachen, A., Pippuri, J. and Arkkio, A. (2010), 'Interdependence of hysteresis and eddy-current losses in laminated magnetic cores of electrical machines', *IEEE Trans. Magn.* **46**(2), 306–309.
- Dlala, E., Saitz, J. and Arkkio, A. (2006), 'Inverted and forward Preisach models for numerical analysis of electromagnetic field problems', *IEEE Trans. Magn.* **42**(8), 1963–1973.

- Du, Y., Cheng, Z., Zhang, J., Liu, L., Fan, Y., Wu, W., Zhai, Z. and Wang, J. (2009), Additional iron loss modeling inside silicon steel laminations, in 'IEEE International Electric Machines and Drives Conference (IEMDC)', Miami, FL, USA, May 2009, pp. 826–831.
- Dular, P. (2008), 'A time-domain homogenization technique for lamination stacks in dual finite element formulations', *J. Comp. Appl. Math.* **215**, 390–399.
- Dular, P., Gyselinck, J., Geuzaine, C., Sadowski, N. and Bastos, J. (2003), 'A 3-D magnetic vector potential formulation taking eddy currents in lamination stacks into account', *IEEE Trans. Magn.* **39**(3), 1424–1427.
- Dupré, L., Bertotti, G. and Melkebeek, J. (1998), 'Dynamic Preisach model and energy dissipation in soft magnetic materials', *IEEE Trans. Magn.* **34**(4), 1168–1170.
- Dupré, L., Gyselinck, J. and Melkebeek, J. (1998), 'Complementary finite element methods in 2D magnetics taking into account a vector Preisach model', *IEEE Trans. Magn.* **34**(5), 3048–3051.
- Emery, R. and Eugene, J. (2002), 'Harmonic losses in LCI-fed synchronous motors', *IEEE Trans. Ind. Appl.* **38**(4), 948–954.
- EN ISO 5176-1 (2003), *Measurement of fluid flow by means of pressure differential devices inserted in circular cross-section conduits running full - Part 1: General principles and requirements*, EN ISO, Brussels, Belgium.
- EN ISO 5176-2 (2003), *Measurement of fluid flow by means of pressure differential devices inserted in circular cross-section conduits running full - Part 2: Orifice plates*, EN ISO, Brussels, Belgium.
- Englebretson, S. C. (2009), Induction Machine Stray Loss from Inter-bar Currents, PhD thesis, Massachusetts Institute of Technology, Cambridge, MA, USA.
- Fiorillo, F. and Novikov, A. (1990), 'An improved approach to power losses in magnetic laminations under nonsinusoidal induction waveform', *IEEE Trans. Magn.* **26**(5), 2904–2910.
- Fonteyn, K. and Belahcen, A. (2008), Numerical and experimental results from a vertical yoke system for measuring magnetic properties of Fe-Si steel sheets, in 'International Conference on Electrical Machines and Systems (ICEMS)', Wuhan, China, October 2008, pp. 434–438.
- Gibbs, W. (1947), 'Tooth-ripple losses in unwound pole-shoes', *J. Inst. Electr. Eng. II* **94**(37), 2–12.
- Graham, C. D. (1982), 'Physical origin of losses in conducting ferromagnetic materials (invited)', *J. Appl. Phys.* **53**(11), 8276–8280.
- Greig, J. and Mukherji, K. (1957), 'An experimental investigation of tooth-ripple flux pulsations in smooth laminated pole-shoes', *Proc. IEE C* **104**(6), 332–338.
- Guerra, F. C. F. and Mota, W. S. (2007), 'Magnetic core model', *IET Sci. Meas. Technol.* **1**(3), 145–151.

- Gyselinck, J. and Dular, P. (2004), 'A time-domain homogenization technique for laminated iron cores in 3-D finite-element models', *IEEE Trans. Magn.* **40**(2), 856–859.
- Gyselinck, J., Dular, P., Sadowski, N., Leite, J. and Bastos, J. (2004), 'Incorporation of a Jiles-Atherton vector hysteresis model in 2D FE magnetic field computations: Application of the Newton-Raphson method', *COMPEL* **23**(3), 685–693.
- Gyselinck, J., Geuzaine, C. and Sabariego, R. (2011), Considering laminated cores and eddy currents in 2D and 3D finite element simulation of electrical machines, in '18th Conference on the Computation of Electromagnetic Fields (COMPUMAG)', Sydney, Australia, July 2011.
- Gyselinck, J., Sabariego, R. and Dular, P. (2006), 'A nonlinear time-domain homogenization technique for laminated iron cores in three-dimensional finite-element models', *IEEE Trans. Magn.* **42**(4), 763–766.
- Gyselinck, J., Vandeveld, L., Makaveev, D. and Melkebeek, J. (2000), 'Calculation of no load losses in an induction motor using an inverse vector Preisach model and an eddy current loss model', *IEEE Trans. Magn.* **36**(4), 856–860.
- Gyselinck, J., Vandeveld, L., Melkebeek, J., Dular, P., Henrotte, F. and Legros, W. (1999), 'Calculation of eddy currents and associated losses in electrical steel laminations', *IEEE Trans. Magn.* **35**(3), 1191–1194.
- Hargreaves, P., Mecrow, B. and Hall, R. (2011), Calculation of iron loss in electrical generators using finite element analysis, in 'IEEE International Electric Machines Drives Conference (IEMDC), Niagara Falls, ON, Canada, May 2011', pp. 1368–1373.
- Hatua, K., Jain, A., Banerjee, D. and Ranganathan, V. (2012), 'Active damping of output LC filter resonance for vector-controlled VSI-fed AC motor drives', *IEEE Trans. Ind. Electr.* **59**(1), 334–342.
- Huang, Y., Dong, J., Zhu, J. and Guo, Y. (2012), 'Core loss modeling for permanent-magnet motor based on flux variation locus and finite-element method', *IEEE Trans. Magn.* **48**(2), 1023–1026.
- IEC/EN 60034-2 (2007), *Rotating electrical machines, Part 2: Methods for determining losses and efficiency of rotating electrical machinery from tests (excluding machines for traction vehicles)*, IEC, Geneva, Switzerland.
- IEC/EN 60034-2A (1974), *Rotating electrical machines, Part 2A: Methods for determining losses and efficiency of rotating electrical machinery from tests (excluding machines for traction vehicles) Measurement of losses by the calorimetric method*, IEC, Geneva, Switzerland.
- IEEE Std 112 (2004), *IEEE Guide for Test Procedures for Synchronous Machines*, IEEE, New York, NY, USA.
- IEEE Std 115 (1994), *IEEE Guide for Test Procedures for Synchronous Machines*, IEEE, New York, NY, USA.
- Islam, M. J. (2010), Finite-element analysis of eddy currents in the form-wound multi-conductor windings of electrical machines, PhD thesis, Helsinki University of Technology, Espoo, Finland.

- Itoh, J.-I. and Ogura, T. (2010), Evaluation of total loss for an inverter and motor by applying modulation strategies, in '14th International Power Electronics and Motion Control Conference (EPE/PEMC)', Ohrid, Macedonia, September 2010, pp. 21–28.
- Jalilian, A., Gosbell, V., Perera, B. and Cooper, P. (1999), 'Double chamber calorimeter (DCC): a new approach to measure induction motor harmonic losses', *IEEE Trans. Energy Convers.* **14**(3), 680–685.
- Jiles, D. and Atherton, D. (1986), 'Theory of ferromagnetic hysteresis (invited)', *J. Appl. Phys.* **55**, 2115–2120.
- Jiles, D. C. (1994), 'Frequency dependence of hysteresis curves in conducting magnetic materials', *J. Appl. Phys.* **76**(10), 5849–5855.
- Karmaker, H. (1982), 'Open circuit tooth ripple losses in slotted laminated poles of electrical machines with amortisseur windings', *IEEE Trans. Power App. Syst.* **PAS-101**(5), 1122–1128.
- Karmaker, H. (1992), 'Stray losses in large synchronous machines', *IEEE Trans. Energy Convers.* **7**(1), 148–153.
- Karmaker, H. and Knight, A. (2005), 'Investigation and simulation of fields in large salient-pole synchronous machines with skewed stator slots', *IEEE Trans. Energy Convers.* **20**(3), 604–610.
- Knight, A., Milliband, P., Leong, C. and McMahon, R. (2005), Power losses in small inverter-fed induction motors, in 'IEEE International Conference on Electric Machines and Drives', San Antonio, TX, USA, May, 2005, pp. 601–607.
- Knight, A., Salmon, J. and Ewanchuk, J. (2011), A simple method to account for PWM eddy current iron losses in finite element analysis, in 'The Third Annual IEEE Energy Conversion Congress and Exposition (ECCE)', Phoenix, AZ, USA, September 2011, pp. 441–448.
- Knight, A., Troitskaia, S., Stranges, N. and Merkhof, A. (2009a), 'Analysis of large synchronous machines with axial skew, part 1: flux density and open-circuit voltage harmonics', *IET Electr. Power Appl.* **3**(5), 389–397.
- Knight, A., Troitskaia, S., Stranges, N. and Merkhof, A. (2009b), 'Analysis of large synchronous machines with axial skew, part 2: inter-bar resistance, skew and losses', *IET Electr. Power Appl.* **3**(5), 398–406.
- Knight, A. and Zhan, Y. (2008), 'Identification of flux density harmonics and resulting iron losses in induction machines with nonsinusoidal supplies', *IEEE Trans. Magn.* **44**(6), 1562–1565.
- Krah, J., Bergqvist, A. and Engdahl, G. (2002), 'Homogenization algorithms for calculation of field quantities in laminated magnetic materials', *IEEE Trans. Magn.* **38**(5), 2385–2387.
- Krasnoselskii, M. and Pokrovskii, A. (1983), *Systems with Hysteresis*, Nauka.
- Kuczmann, M. (2009), 'Measurement and simulation of vector hysteresis characteristics', *IEEE Trans. Magn.* **45**(11), 5188–5191.
- Lammeraner, J. and Štafl, M. (1964), *Eddy Currents*, Iliffe Books.

- Lederer, D., Igarashi, H., Kost, A. and Honma, T. (1999), 'On the parameter identification and application of the Jiles-Atherton hysteresis model for numerical modelling of measured characteristics', *IEEE Trans. Magn.* **35**(3), 1211–1214.
- Leite, J., Benabou, A., Sadowski, N. and da Luz, M. (2009), 'Finite element three-phase transformer modeling taking into account a vector hysteresis model', *IEEE Trans. Magn.* **45**(3), 1716–1719.
- Leite, J., Sadowski, N., Kuo-Peng, P., Batistela, N. and Bastos, J. (2003), 'The inverse Jiles-Atherton model parameters identification', *IEEE Trans. Magn.* **39**(3), 1397–1400.
- Leite, J., Sadowski, N., Kuo-Peng, P., Batistela, N., Bastos, J. and de Espindola, A. (2004), 'Inverse Jiles-Atherton vector hysteresis model', *IEEE Trans. Magn.* **40**(4), 1769–1775.
- Li, J., Choi, D.-W., Cho, C.-H., Koo, D.-H. and Cho, Y.-H. (2011), 'Eddy-current calculation of solid components in fractional slot axial flux permanent magnet synchronous machines', *IEEE Trans. Magn.* **47**(10), 4254–4257.
- Lin, D., Zhou, P., Fu, W., Badics, Z. and Cendes, Z. (2004), 'A dynamic core loss model for soft ferromagnetic and power ferrite materials in transient finite element analysis', *IEEE Trans. Magn.* **40**(2), 1318–1321.
- Lin, R. (2010), *Electromagnetic and Mechanical Finite Element Analysis of End Region of Large-Sized Three-Phase Squirrel-Cage Induction Machines*, PhD thesis, Aalto University School of Science and Technology, Espoo, Finland.
- Lindström, J. (1994), *Calorimetric methods for loss measurements of small cage induction motors*, Master's thesis, Helsinki University of Technology, Espoo, Finland.
- Liu, H., Xu, L. and Shangguan, M. (2011), Finite element method simulation of a high speed wound-rotor synchronous machine, in 'International Conference on Electrical Machines and Systems (ICEMS)', Beijing, China, August 2011, pp. 1–4.
- Mademlis, C., Margaritis, N. and Xypteras, J. (2000), 'Magnetic and thermal performance of a synchronous motor under loss minimization control', *IEEE Trans. Energy Convers.* **15**(2), 135–142.
- Mademlis, C., Xypteras, J. and Margaritis, N. (1998), 'Loss minimization in wound-field cylindrical rotor synchronous motor drives', *IEEE Trans. Power Electr.* **13**(2), 288–296.
- Magnet-Physik (2008), *REMAGRAPH[®] C - 500 (data sheet)*, Magnet-Physik Dr. Steingroever GmbH.
- Mathekga, M., McMahon, R. and Knight, A. (2011), 'Application of the fixed point method for solution in time stepping finite element analysis using the inverse vector Jiles-Atherton model', *IEEE Trans. Magn.* **47**(10), 3048–3051.
- Mayergoyz, I. (1986), 'Mathematical models of hysteresis', *IEEE Trans. Magn.* **22**(5), 603–608.
- Mayergoyz, I. (1988a), 'Dynamic Preisach models of hysteresis', *IEEE Trans. Magn.* **24**(6), 2925–2927.

- Mayergoyz, I. D. (1988b), 'Vector Preisach hysteresis models (invited)', *J. Appl. Phys.* **63**(8), 2995–3000.
- Mayergoyz, I. and Serpico, C. (1999), 'Nonlinear diffusion of electromagnetic fields and excess eddy current losses', *J. Appl. Phys.* **85**(8), 4910–4912.
- Mei, W., Jabbar, M. and Tay, A. (2001), Determination of thermal performance of small electric motors, in '4th IEEE International Conference on Power Electronics and Drive Systems', Vol. 2, Denpasar, Indonesia, October 2001, pp. 877–880.
- Merkhouf, A., Hudon, C., Belec, M., Guillot, E., Aguiar, A. and Al-Haddad, K. (2011), Electromagnetic losses computation in existing large hydro electrical generators, in 'IEEE International Electric Machines Drives Conference (IEMDC)', Niagara Falls, ON, Canada, May 2011, pp. 113–118.
- Overshott, K., Preece, I. and Thompson, J. (1968), 'Magnetic properties of grain-oriented silicon iron. Part 2: Basic experiments on the nature of the anomalous loss using an individual grain', *Proc. IEE* **115**(12), 1840–1845.
- Park, J.-D., Kalev, C. and Hofmann, H. (2008), 'Analysis and reduction of time harmonic rotor loss in solid-rotor synchronous reluctance drive', *IEEE Trans. Power Electr.* **23**(2), 985–992.
- Permiakov, V., Dupre, L., Pulnikov, A. and Melkebeek, J. (2004), 'Loss separation and parameters for hysteresis modelling under compressive and tensile stresses', *J. Magn. Magn. Mater.* **272-276**, 553–554.
- Pippuri, J. (2010), Finite Element Analysis of Eddy Current Losses in Steel Laminations of Inverter-Fed Electrical Machines, PhD thesis, Aalto University School of Science and Technology, Espoo, Finland.
- Pluta, W. (2010), 'Some properties of factors of specific total loss components in electrical steel', *IEEE Trans. Magn.* **46**(2), 322–325.
- Preis, K., Biro, O. and Ticar, I. (2005), 'FEM analysis of eddy current losses in nonlinear laminated iron cores', *IEEE Trans. Magn.* **41**(5), 1412–1415.
- Preisach, F. (1935), 'Loss separation in nonoriented electrical steels', *Zeitschrift für Physik* **94**, 277–302.
- Rasilo, P., Singh, D., Belahcen, A. and Arkkio, A. (2012), Iron losses, magnetoelasticity and magnetostriction in ferromagnetic steel laminations, in 'The 15th Biennial IEEE Conference on Electromagnetic Field Computation (CEFC)', Oita, Japan, November 2012.
- Richardson, P. (1945), 'Stray losses in synchronous electrical machinery', *J. Inst. Electr. Eng. II* **92**(28), 291–301.
- Righi, L., Koltermann, P., Sadowski, N., Bastos, J., Carlson, R., Kost, A., Janicke, L. and Lederer, D. (2000), 'Non-linear magnetic field analysis by FEM using Langevin function', *IEEE Trans. Magn.* **36**(4), 1263–1266.
- Righi, L., Sadowski, N., Carlson, R., Bastos, J. and Batislska, N. (2001), 'A new approach for iron losses calculation in voltage fed time stepping finite elements', *IEEE Trans. Magn.* **37**(5), 3353–3356.

- Sabariego, R., Dular, P. and Gyselinck, J. (2008), 'Time-domain homogenization of windings in 3-D finite element models', *IEEE Trans. Magn.* **44**(6), 1302–1305.
- Sadowski, N., Batistela, N., Bastos, J. and Lajoie-Mazenc, M. (2002), 'An inverse Jiles-Atherton model to take into account hysteresis in time-stepping finite-element calculations', *IEEE Trans. Magn.* **38**(2), 797–800.
- Schmidt, E., Traxler-Samek, G. and Schwery, A. (2005), Influence of higher harmonics in the end region magnetic field on eddy currents in the stator clamping system of hydro generators, in 'IEEE International Conference on Electric Machines and Drives (IEMDC)', San Antonio, TX, USA, May, 2005, pp. 1268–1274.
- Shisha, S. (2008), Analysis of Inverter-Fed Losses on the Solid Rotor of Large-scale Synchronous Machines, Licentiate thesis, Royal Institute of Technology (KTH), Stockholm, Sweden.
- Shisha, S. and Sadarangani, C. (2009), Evaluation of zero vectors in DTC control of synchronous machines and its effect on losses, in 'IEEE Energy Conversion Congress and Exposition (ECCE)', San Jose, CA, USA, September 2009, pp. 2552–2556.
- Shisha, S., Sadarangani, C. and Nee, H.-P. (2012), 'Loss distribution on solid pole plates of wound-rotor synchronous motors fed from inverters using direct torque control', *IEEE Trans. Energy Convers.* **27**(1), 63–70.
- Silva, V., Meunier, G. and Foggia, A. (1995), 'A 3-D finite-element computation of eddy currents and losses in laminated iron cores allowing for electric and magnetic anisotropy', *IEEE Trans. Magn.* **31**(3), 2139–2141.
- Spooner, T. and Kinnard, I. F. (1924), 'Surface iron losses with reference to laminated materials', *Am. Inst. Electr. Eng. Trans.* **XLIII**, 262–281.
- Steinmetz, C. P. (1892), 'On the law of hysteresis', *Am. Inst. Electr. Eng. Trans.* **9**, 3–64. Reprinted in Proc. IEEE 72 (2), 197–221 (1984).
- Stermecki, A., Biro, O., Bakhsh, I., Rainer, S., Ofner, G. and Ingruber, R. (2012), '3-D finite element analysis of additional eddy current losses in induction motors', *IEEE Trans. Magn.* **48**(2), 959–962.
- Stoleriu, L., Andrei, P. and Stancu, A. (2008), 'First order reversal curves identification procedures for vector models of hysteresis', *J. Appl. Phys.* **103**(7), 1–3.
- Stranges, N. and Dymond, J. (2003), 'How design influences the temperature rise of motors on inverter drives', *IEEE Trans. Ind. Appl.* **39**(6), 1584–1591.
- Sun, P., Lai, J., Liu, C. and Yu, W. (2012), 'A 55kW three-phase inverter based on hybrid-switch soft-switching modules for high temperature hybrid electric vehicle drives application', *IEEE Trans. Ind. Appl.* **48**(3), 962–969.
- Szabados, B. and Mihalcea, A. (2002), 'Design and implementation of a calorimetric measurement facility for determining losses in electrical machines', *IEEE Trans. Instrum. Meas.* **51**(5), 902–907.

- Traxler-Samek, G. and Ardley, G. (2009), Iron losses in salient-pole synchronous machines considering unidirectional and elliptic magnetization, in '8th International Symposium on Advanced Electromechanical Motion Systems (ELECTROMOTION)', Lille, France, July 2009, pp. 1–6.
- Traxler-Samek, G., Lugand, T. and Schwery, A. (2010), 'Additional losses in the damper winding of large hydrogenerators at open-circuit and load conditions', *IEEE Trans. Ind. Electr.* **57**(1), 154–160.
- Traxler-Samek, G., Zickermann, R. and Schwery, A. (2008), Advanced calculation of temperature rises in large air-cooled hydro-generators, in 'International Conference on Electrical Machines (ICEM)', Vilamoura, Portugal, September 2008, pp. 1–6.
- Traxler-Samek, G., Zickermann, R. and Schwery, A. (2010), 'Cooling airflow, losses, and temperatures in large air-cooled synchronous machines', *IEEE Trans. Ind. Electr.* **57**(1), 172–180.
- Turner, D. R., Binns, K. J., Shamsadeen, B. N. and Warne, D. F. (1991), 'Accurate measurement of induction motor losses using balance calorimeter', *IEE Proc. B* **138**(5), 233–242.
- Vetter, W. and Reichert, K. (1994), 'Determination of damper winding and rotor iron currents in convertor- and line-fed synchronous machines', *IEEE Trans. Energy Convers.* **9**(4), 709–716.
- Villar, I., Rufer, A., Viscarret, U., Zurkinden, F. and Etxeberria-Otadui, I. (2008), Analysis of empirical core loss evaluation methods for non-sinusoidally fed medium frequency power transformers, in 'IEEE International Symposium on Industrial Electronics (ISIE)', Cambridge, UK, June–July 2008, pp. 208–213.
- Weier, S., McMahon, R. and Malliband, P. (2006), Calorimetry for power electronics, in 'Proceedings of the 41st International Universities Power Engineering Conference', Vol. 2, Newcastle upon Tyne, UK, September 2006, pp. 608–612.
- Weiss, J. and Stephens, C. (1981), 'Finite elements for three-dimensional magnetostatic fields and its application to turbine-generator end regions', *IEEE Trans. PAS* **PAS-100**(4), 1591–1596.
- Wu, Y., McMahon, R., Zhan, Y. and Knight, A. (2006), Impact of PWM schemes on induction motor losses, in 'IEEE Industry Applications Conference', Vol. 2, Tampa, FL, USA, October, 2006, pp. 813–818.
- Wu, Y., Shafi, M., Knight, A. and McMahon, R. (2011), 'Comparison of the effects of continuous and discontinuous PWM schemes on power losses of voltage-sourced inverters for induction motor drives', *IEEE Trans. Power Electr.* **26**(1), 182–191.
- Wu, Y., Shao, S., McMahon, R., Zhan, Y. and Knight, A. (2008), Power loss study of inverter-fed machine drives using discontinuous pulse width modulation, in 'IEEE International Conference on Sustainable Energy Technologies (ICSET)', Singapore, November, 2008, pp. 1172–1177.
- Yamazaki, K. and Fukushima, N. (2010), 'Iron-loss modeling for rotating machines: Comparison between Bertotti's three-term expression and 3-D eddy-current analysis', *IEEE Trans. Magn.* **46**(8), 3121–3124.

- Yamazaki, K. and Fukushima, N. (2011), 'Torque and loss calculation of rotating machines considering laminated cores using post 1-D analysis', *IEEE Trans. Magn.* **47**(5), 994–997.
- Zhan, Y., Knight, A. and Stranges, N. (2009), 'Multislice inter-bar model for large synchronous machines with skewed stator slots', *IEEE Trans. Magn.* **45**(3), 1800–1803.
- Zhan, Y., Knight, A., Wu, Y. and McMahon, R. (2008), Investigation and comparison of inverter-fed induction machine loss, in 'IEEE Industry Applications Society Annual Meeting', Edmonton, AB, Canada, October, 2008, pp. 1–6.
- Zhang, H., Cao, W., Zanchetta, P. and Li, J. (2011), Thermal analysis of a balanced calorimeter for testing electrical machines, in 'The Third Annual IEEE Energy Conversion Congress and Exposition (ECCE)', Phoenix, AZ, USA, September 2011, pp. 429–432.
- Zhang, H., Zanchetta, P., Gerada, C., Cao, W. and Bradley, K. (2010), Design of a calorimeter for induction machine efficiency measurement by CFD modeling, in '36th Annual Conference on IEEE Industrial Electronics Society', Phoenix, AZ, USA, November 2010, pp. 817–822.
- Zhou, Y. and Hu, Y. (2008), A novel direct torque control for electrically excited synchronous motor drives with high power factor and low ripples in flux and torque, in 'Annual IEEE Power Electronics Specialists Conference (PESC)', Rhodes, Greece, June 2008, pp. 4752–4756.
- Zirka, S., Moroz, Y., Marketos, P. and Moses, A. (2006), 'Viscosity-based magnetodynamic model of soft magnetic materials', *IEEE Trans. Magn.* **42**(9), 2121–2132.
- Zirka, S., Moroz, Y., Marketos, P. and Moses, A. (2010), 'Loss separation in nonoriented electrical steels', *IEEE Trans. Magn.* **46**(2), 286–289.

Publication Errata

Publication II

The excess-loss coefficient in the last paragraph of Section 4.1 should be divided with the mass density ρ . The correct expression is $\rho^{-1}(\sigma GV_0 S)^{1/2} = 9.39 \times 10^{-5}(\text{W/kg})(\text{s/T})^{3/2}$.

Equation (37) should be replaced by the expression currently on the left-hand side of the equation.

Publication III

The last word on the line following Equation (26) should be 'of' instead of 'or'.

Publication IV

In Fig. 13, "Hysteretic materials" are depicted by a solid line instead of a dashed-dotted line, unlike mentioned in the legend.

